RSC Advances

PAPER

View Article Online
View Journal | View Issue

Open Access Article. Published on 10 February 2026. Downloaded on 2/17/2026 2:53:54 PM.
This article is licensed under a Creative Commons Attribution-NonCommercial 3.0 Unported Licence.

Check for updates

Cite this: *RSC Adv.*, 2026, **16**, 8072

Determination of the structure and dynamics of linear polypeptide gramicidin A at atomic-scale resolution

Bijay Laxmi Pradhan,[ab] Prince Sen,[c] Adarsh Kumar,[c] Anirban Bhunia,[d] Krishna Kishor Dey*[c] and Manasi Ghosh*[b]

The resonance lines of the ^{1}H and ^{13}C liquid NMR spectra of the linear peptide antibiotic gramicidin A were assigned by performing various 2D NMR experiments such as 2D ^{1}H–^{13}C HSQC, 2D ^{1}H–^{15}N HSQC, ^{1}H–^{13}C HMBC, ^{1}H–^{1}H COSY, and ^{1}H–^{1}H TOCSY. The spatial proximity among various protons and inter-nuclear distances were determined by a 2D ^{1}H–^{1}H NOESY NMR experiment. The detailed structure and nuclear spin dynamics of this peptide antibiotic were also determined by extracting the principal components of CSA (chemical shift anisotropy) parameters and spin-lattice relaxation times at the various ^{13}C nuclear sites by applying advanced solid-state NMR methodologies. The CSA parameters were determined by employing a ^{13}C 2DPASS CP-MAS SSNMR experiment; the site-specific spin-lattice relaxation time was determined by a method designed by Torchia, and the spatial proximity between ^{1}H and ^{13}C nuclei was determined by a ^{1}H–^{13}C PMLG HETCOR experiment. A higher degree of freedom was observed within this linear polypeptide by the spin-lattice relaxation measurements, which can be considered the origin of its antibacterial activity. The principal components of the CSA-parameters are substantially higher for the carbon-13 nuclei residing on the indole ring of the l-tryptophan amino acid residue due to magnetic shielding and deshielding effects and also due to the presence of intramolecular and intermolecular hydrogen bonds. Notably, ^{13}C nuclei in the indole rings of l-tryptophan residues exhibited significantly larger values of the principal components of CSA parameters and longer spin-lattice relaxation times. These types of detailed analysis of the structure and dynamics of peptide antibiotics will augment the field of 'NMR crystallography' and will also serve as a foundation for formulating a new class of antimicrobial peptides.

Received 27th November 2025
Accepted 21st January 2026

DOI: 10.1039/d5ra09180b

rsc.li/rsc-advances

1. Introduction

Antibiotic resistance poses a major global health challenge as conventional antibiotics that target specific intracellular components can rapidly lose efficacy due to minor structural changes or bacterial defense mechanisms such as reduced membrane permeability and drug efflux. To address this issue, attention has shifted toward antimicrobial peptides (AMPs), which have served as natural defense molecules for millions of years with minimal resistance development. Unlike traditional antibiotics, AMPs primarily disrupt bacterial membranes rather than binding to specific intracellular targets, making resistance development more difficult. Moreover, AMPs exhibit broad bioactivity against bacteria, viruses, fungi, parasites, insects, and cancer cells.[1–9]

Gramicidin A, a well-known AMP discovered in 1939 from *Bacillus brevis*, was the first antibiotic produced commercially and remains a potent broad-spectrum agent, particularly against Gram-positive and multidrug-resistant bacteria.[10–14] However, its high hemolytic activity restricts its clinical use to topical applications for localized infections of the skin, eyes, nose, and throat.[15] Beyond its antimicrobial role, gramicidin A has also shown notable cytotoxicity toward cancer cells, suggesting potential anticancer applications.[16]

Structurally, gramicidin A is a highly hydrophobic, linear pentadecapeptide with alternating L- and D-amino acids, forming π (L, D) helices that promote head-to-head dimerization through hydrogen bonding (as it is shown in Fig. 1). This dimer forms a transmembrane ion channel, which allows gramicidin A to be a widely used model system for studying membrane channel structure and dynamics. The peptide's hydrophobic and amphipathic residues, blocked termini, and ability to integrate into lipid bilayers are central to its biological activity.[17–19]

[a]Department of Physics, Institute of Science, Banaras Hindu University, Varanasi-221005, Uttar-Pradesh, India

[b]Physics Section, Mahila Maha Vidyalaya, Banaras Hindu University, Varanasi-221005, Uttar-Pradesh, India. E-mail: manasi.ghosh@bhu.ac.in; manasi.ghosh@gmail.com

[c]Department of Physics, Dr. Harisingh Gour Central University, Sagar-470003, Madhya-Pradesh, India. E-mail: dey.krishna@gmail.com

[d]Department of Chemical Sciences, Bose Institute, Salt Lake, EN 80, Sector V, Kolkata 700091, West-Bengal, India

© 2026 The Author(s). Published by the Royal Society of Chemistry

Open Access Article. Published on 10 February 2026. Downloaded on 2/17/2026 2:53:54 PM.
This article is licensed under a Creative Commons Attribution-NonCommercial 3.0 Unported Licence.

The ^{13}C chemical shifts and spin-lattice relaxation times (T_1) of gramicidin A were first measured by Fossel *et al.* (1974) using solution NMR spectroscopy.[20] Their T_1data indicated that the peptide backbone exhibits the slowest molecular motion, while the N-terminal residues show relatively faster dynamics. In 1998, Per-Ola Quist obtained the ^{13}C CP-MAS solid-state NMR spectrum of gramicidin A incorporated into a lipid membrane;[21] the residual chemical shift tensors, which were consistent with

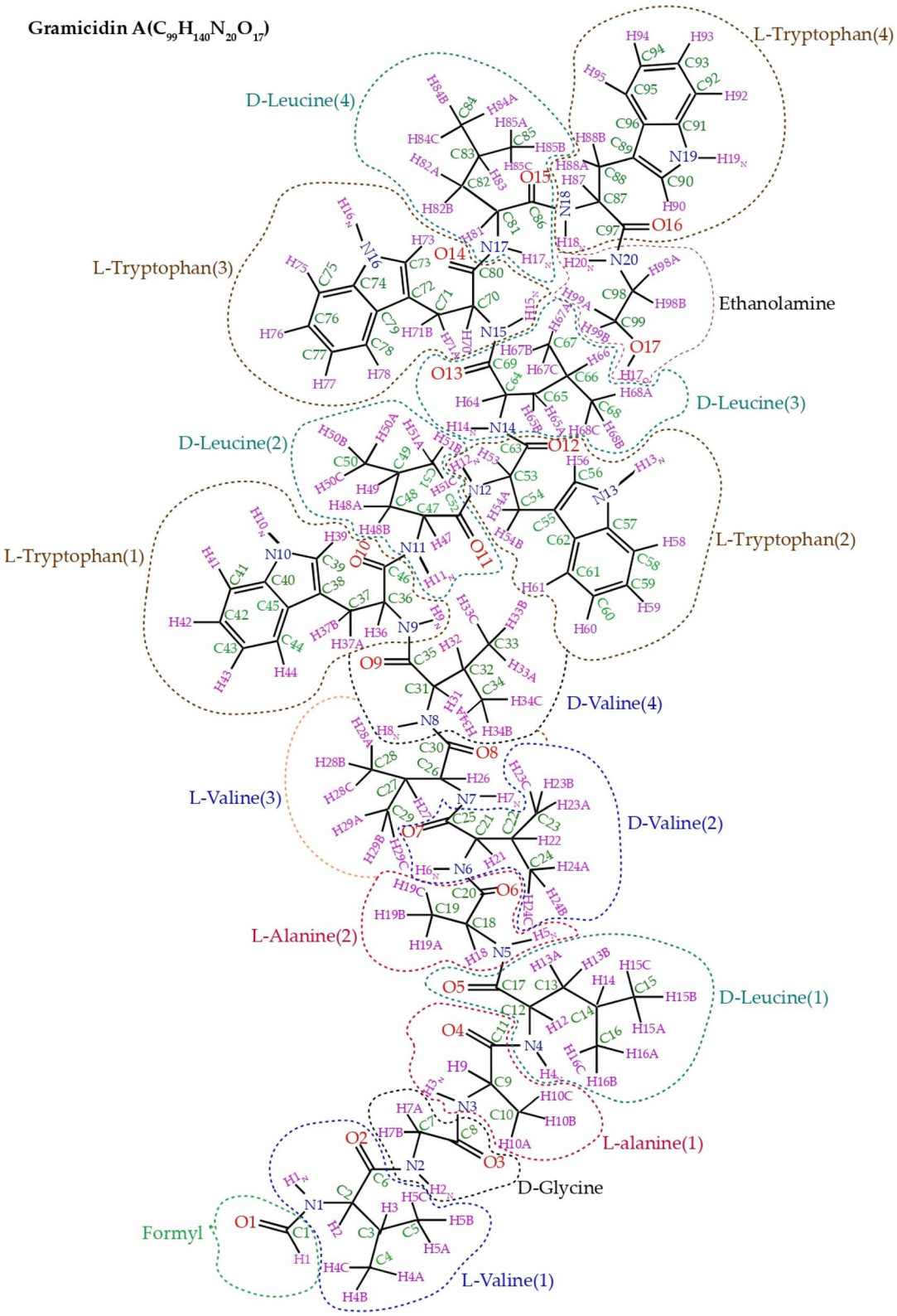

Fig. 1 The amino acid sequence of gramicidin A, where all residues are hydrophobic.

Open Access Article. Published on 10 February 2026. Downloaded on 2/17/2026 2:53:54 PM.
This article is licensed under a Creative Commons Attribution-NonCommercial 3.0 Unported Licence.

a single-stranded, right-handed $\beta^{6\cdot3}$ helical structure, were also determined. Subsequently, Ketchem and co-workers provided a comprehensive description of both the backbone and side-chain conformations of gramicidin A in a lipid bilayer environment using solid-state NMR spectroscopy.[22]

The main purpose of this work is to study the local structure and nuclear spin-dynamics of this antimicrobial peptide by employing solution and solid-state NMR measurements. We aimed to assign ^{1}H and ^{13}C NMR spectra by employing 2D solution NMR correlation experiments like 2D ^{1}H–^{13}C HSQC, 2D ^{1}H–^{15}N HSQC, ^{1}H–^{13}C HMBC, ^{1}H–^{1}H COSY, and ^{1}H–^{1}H TOCSY. Tryptophan, the most hydrophobic among the naturally occurring amino acids, plays a crucial role in the antimicrobial activity of this membrane protein. Its polar NH group enables the formation of both intra- and intermolecular hydrogen bonds. The presence of an aromatic indole ring allows tryptophan to engage in π–π stacking and weak polar interactions. This unique amphipathic nature contributes to its distinctive hydrogen-bonding capabilities and ability to mediate long-range electrostatic interactions. Additionally, the indole group and amphipathic character of tryptophan favor its localization at the membrane interface.[23–26] We aimed to probe the local structure and dynamics of ^{13}C nuclei residing on all the amino acids, particularly on the tryptophan residue, by using ensembles of solid-state NMR experiments, like ^{13}C spin-lattice relaxation measurements by following the method described by Torchia,[27] ^{13}C CP-MAS (cross-polarization magic-angle spinning) SSNMR (solid-state nuclear magnetic resonance) experiments, ^{13}C 2DPASS (two-dimensional phase-adjusted spinning sideband) CP-MAS (cross-polarization magic-angle spinning) ssNMR (solid-state nuclear magnetic resonance) experiments, and ^{1}H–^{13}C HETCOR (heteronuclear correlation) experiments. Previously, we determined the structure and dynamics of the active pharmaceutical ingredients of drugs and polymers by employing these experiments.[28–32]

Sophisticated nuclear magnetic resonance (NMR) methodologies possess the potential to unlock the intricate relationship between the structure and activity of drug molecules, shedding light on the pathway of drug discovery. Moreover, these studies play a crucial role in comprehending the distribution of electrons surrounding a nucleus, various kinds of chemical bonding, and the dynamic behavior of nuclear spins at different regions within the polypeptide. This understanding, in turn, serves as a foundation for formulating highly effective strategies for developing advanced peptide antibiotics. Moreover, the insights gained from these investigations will make significant contributions to the field of "NMR-crystallography," further enriching our understanding of molecular structures and their interactions. NMR crystallography utilizes diverse information obtained through advanced solid-state NMR techniques in combination with computational chemistry. These approaches are especially valuable for those materials where it is challenging to develop sufficiently large single crystals. While single-crystal diffraction methods reveal the overall molecular structure, NMR crystallography goes further by offering insights into both the structure and the dynamics at each crystallographically distinct nuclear site. The objective of this project is

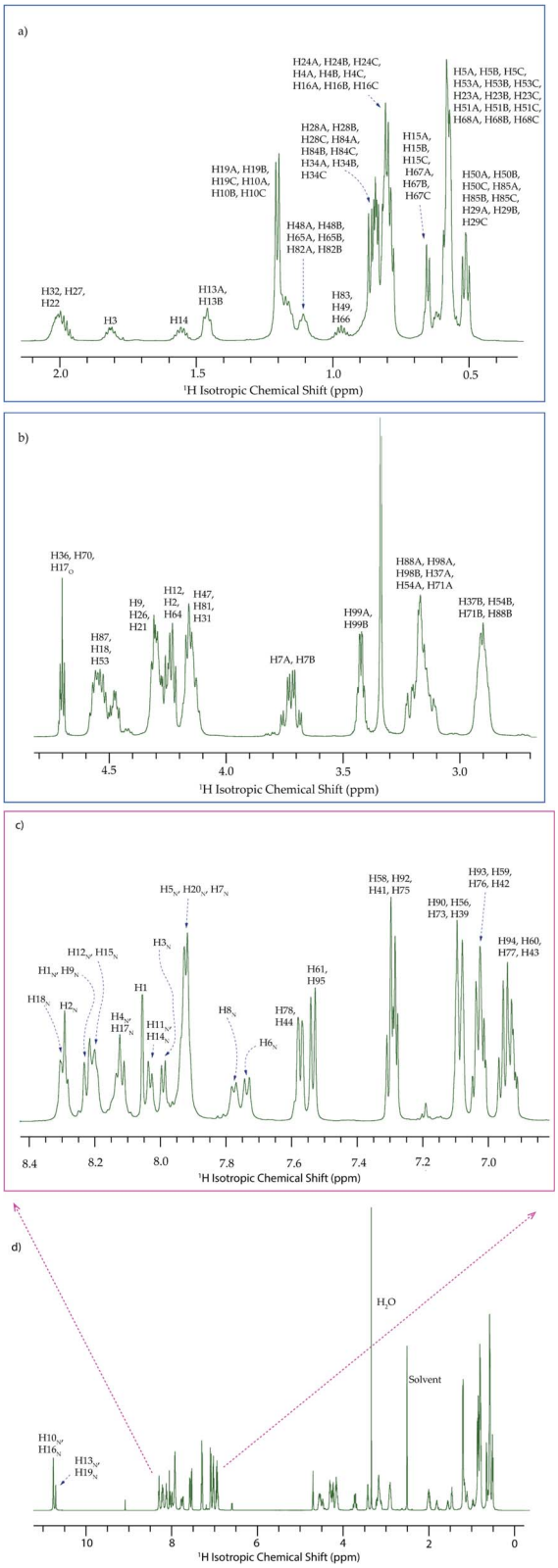

Fig. 2 (d) ^{1}H Liquid NMR spectrum of gramicidin A; (c) assignment of the resonance lines of the ^{1}H liquid NMR spectrum ranging from 8.4 ppm to 6.8 ppm; (b) assignment of the resonance lines of the ^{1}H liquid NMR spectrum in the range from 4.8 ppm to 2.6 ppm; (a) assignment of the resonance lines of the ^{1}H liquid NMR spectrum in the range from 2.1 ppm to 0.4 ppm.

 © 2026 The Author(s). Published by the Royal Society of Chemistry

Open Access Article. Published on 10 February 2026. Downloaded on 2/17/2026 2:53:54 PM.
This article is licensed under a Creative Commons Attribution-NonCommercial 3.0 Unported Licence.

to construct a comprehensive and valuable database for "NMR crystallography" dedicated to peptide antibiotics. This database will provide a wealth of information regarding the structural characteristics and dynamic behavior of AMPs at atomic scale resolution. Such a resource would be of immense significance to researchers and scientists in the fields of pharmaceutical science, drug design, and structure–activity relationship studies. With the establishment of this specialized database, it

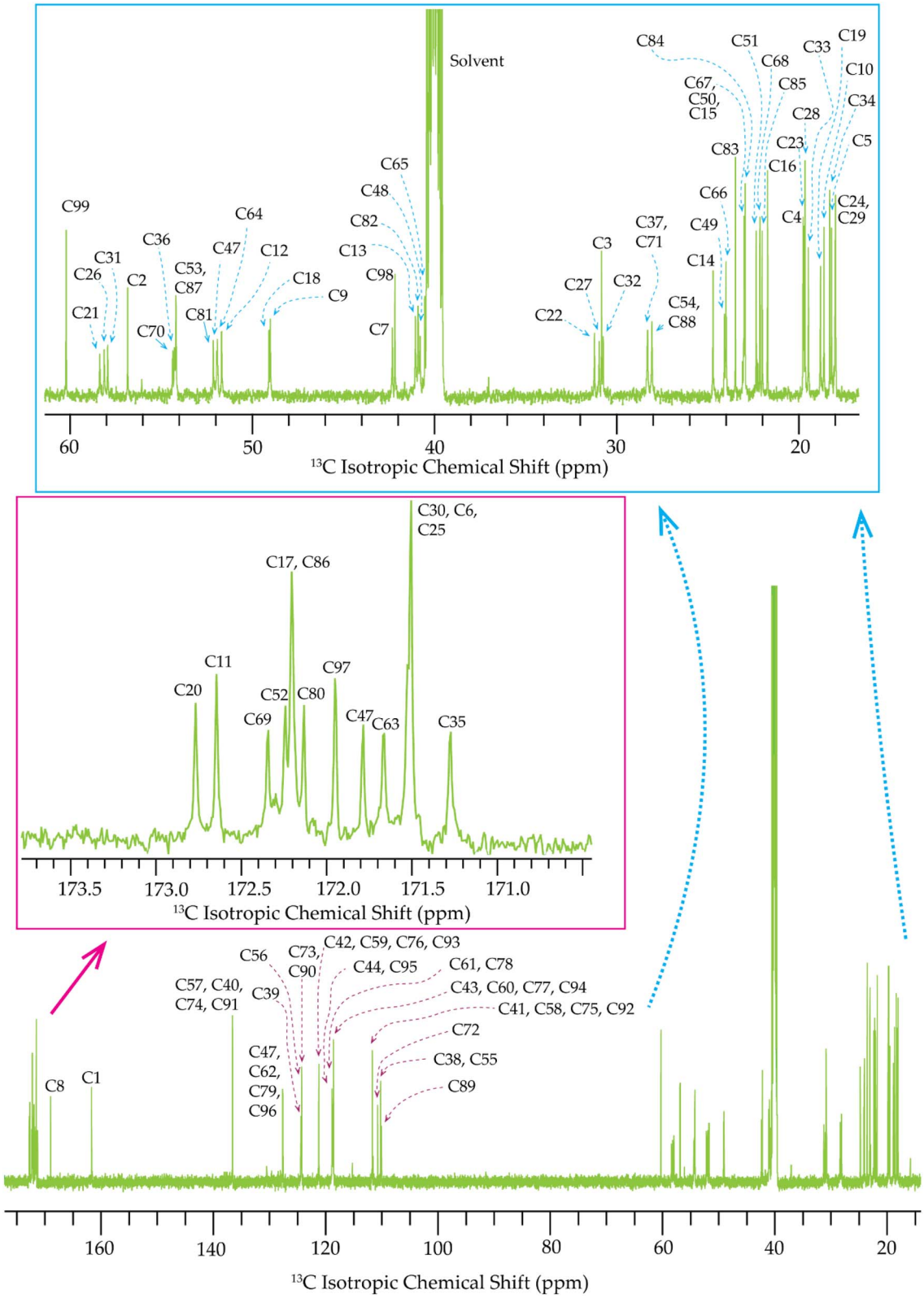

Fig. 3 ^{13}C Liquid NMR spectrum of gramicidin A.

Open Access Article. Published on 10 February 2026. Downloaded on 2/17/2026 2:53:54 PM.
This article is licensed under a Creative Commons Attribution-NonCommercial 3.0 Unported Licence.

is anticipated that it will serve as an indispensable tool for advancing our understanding of AMPs and facilitating more efficient and targeted AMPs.

Though the peptide consists of 15 amino acids, it is made up of only five distinct types: valine, glycine, alanine, leucine, and tryptophan. Additionally, if glycine is considered a potential D residue, the sequence follows an alternating L- and D-pattern. In this structure, the amino acid side chains extend outward, while the carbonyl groups alternate in orientation, pointing up and down within the helix. This unique arrangement forms a hydrophilic pore, facilitating ion transport through the membrane.

2. Experimental

All solid-state NMR (SSNMR) experiments were performed on a JEOL ECX 500 MHz spectrometer equipped with a 3.2 mm JEOL double-resonance MAS probe. The ^{13}C chemical shifts were referenced to the tetramethylsilane (TMS) resonance at 0 ppm. During the ^{13}C CP-MAS SSNMR experiments and 13C spin-lattice relaxation measurements, the magic angle spinning (MAS) speed was maintained at 10 kHz, using a 2 ms contact time, 30 s recycle delay, employing SPINAL-64 for proton decoupling with proton power of 100 kHz. The ^{13}C two-dimensional phase-adjusted spinning sideband (2DPASS) CP-MAS SSNMR experiments[33,34] were carried out at MAS frequencies of 600 Hz and 2 kHz. The MAS frequencies were controlled with high precision by a JEOL commercial MAS controller, maintaining stability at (600 ± 4) Hz and (2000 ± 4) Hz for accuracy and reproducibility. In the present work, the ^{13}C CP-MAS experiment was performed with 32 768 scans, while the ^{13}C 2DPASS CP-MAS experiment required 5200 scans. For determining ^{13}C relaxation times using the Torchia CP method, 2048 scans were recorded. Details of the solid and liquid NMR experiments are described in Section S1 of the SI.

3. Results and discussion

3.1 Accurate assignment of ^{1}H and ^{13}C liquid NMR spectra

The one-dimensional ^{1}H, ^{13}C liquid NMR spectra of gramicidin A are shown in Fig. 2 and 3, respectively. To achieve precise and unambiguous assignments under our experimental conditions, a series of two-dimensional NMR experiments was conducted, including 2D ^{1}H–^{1}H COSY (correlation spectroscopy), 2D ^{1}H–^{1}H TOCSY (total correlation spectroscopy), 2D ^{1}H–^{13}C HSQC (heteronuclear single-quantum coherence), 2D ^{1}H–^{13}C HMBC (heteronuclear multiple–bond correlation), and 2D ^{1}H–^{15}N HSQC (heteronuclear single-quantum coherence). We compared our chemical-shift assignments with those reported in the previously published study by G. E. Hawkes and coauthors.[35] The corresponding datasets are presented in Tables S1 and S2 of the SI. The isotropic chemical shifts assigned to each

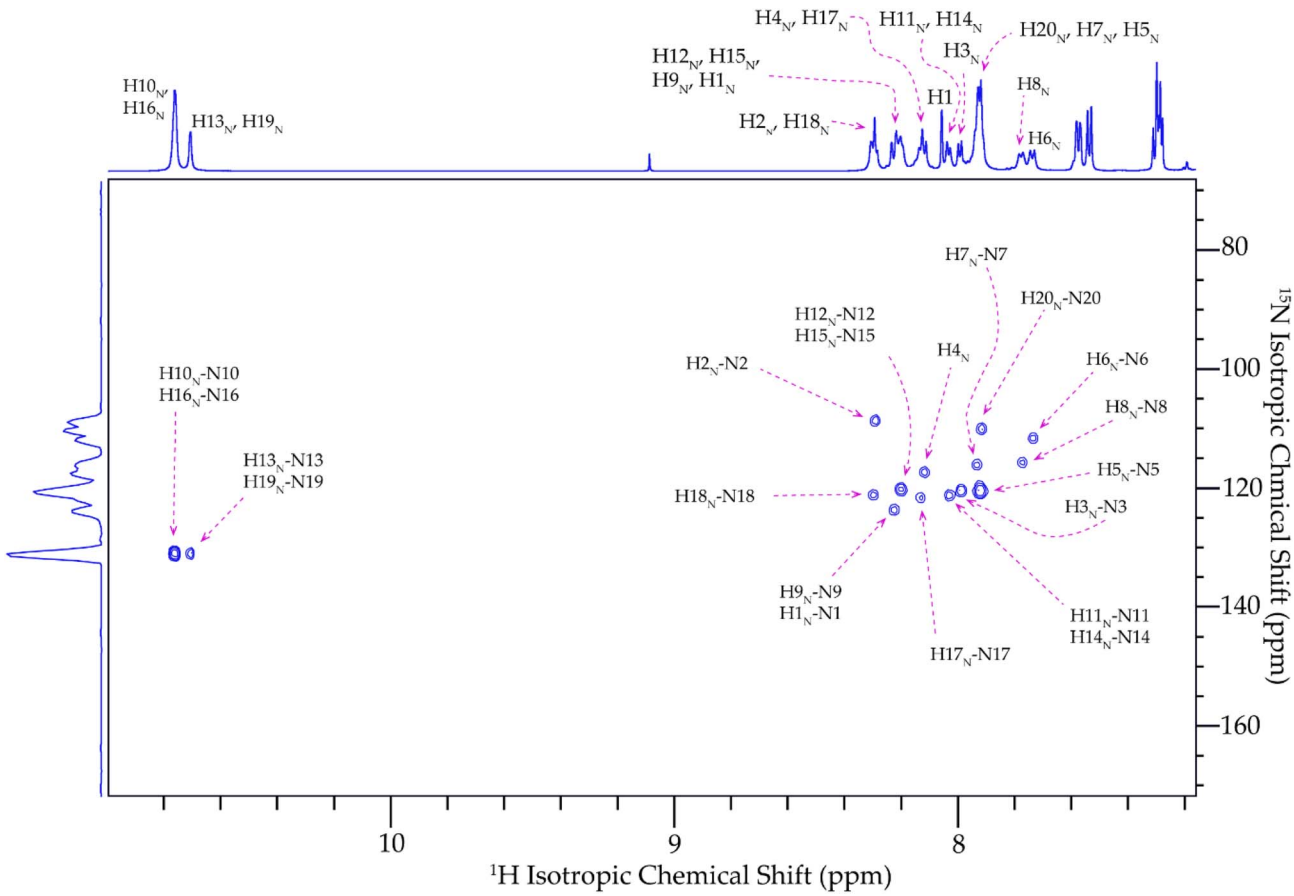

Fig. 4 2D ^{1}H–^{15}N HSQC spectrum of gramicidin A.

 © 2026 The Author(s). Published by the Royal Society of Chemistry

Open Access Article. Published on 10 February 2026. Downloaded on 2/17/2026 2:53:54 PM.
This article is licensed under a Creative Commons Attribution-NonCommercial 3.0 Unported Licence.

^{1}H and ^{13}C nucleus show excellent agreement with the earlier work, exhibiting a linear correlation as illustrated in Fig. S1 and S2 of the SI. The finalized ^{1}H and ^{13}C chemical-shift assignments derived from our analysis are provided in Tables S3 and S4, respectively, of the SI.

Protons that are connected to nitrogen by a direct single bond were distinguished by using 2D ^{1}H–^{15}N HSQC NMR spectra, as shown in Fig. 4 and Table 1. The assignment of both ^{1}H nuclei bonded to nitrogen and the corresponding ^{15}N nuclei was performed by following the previously reported article by G.E. Hawkes and coworkers.[35] It was observed that protons bonded to electronegative nitrogen atoms exhibit relatively downfield chemical shifts, ranging from 7.73 ppm to 10.76 ppm. Notably, the highest chemical shift values of 10.71 ppm and 10.76 ppm were attributed to protons located within the indole rings of tryptophan residues.

The assignment of cross peaks in the 2D ^{1}H–^{13}C HSQC spectrum (Fig. S5 of the SI), identifying the directly bonded ^{13}C and ^{1}H nuclei,[36] is presented in Table S5 of the SI. Similarly, the assignments from 2D ^{1}H–^{13}C HMBC spectra (Fig. S6 of the SI), which provide correlations between ^{1}H and ^{13}C nuclei separated by two to four bonds within the spin system,[37] are presented in Table S6 of the SI. The 2D ^{1}H–^{1}H COSY spectrum of gramicidin A (Fig. S7 of the SI) reveals correlations between vicinal and geminal protons, facilitating the identification of short-range proton connectivity within the molecule.[38] The corresponding assignments are listed in Table S7 of the SI. On the other hand, the 2D ^{1}H–^{1}H TOCSY NMR spectrum (Fig. S8 of the SI) captures through-bond correlations among protons within the same spin system, including those separated by up to six bonds.[39] The proton assignments derived from the TOCSY data are compiled in Table S8 of the SI.

3.2 Analysis of the 2D ^{1}H–^{1}H NOESY NMR spectra of gramicidin A

^{1}H–^{1}H NOESY experiments were performed at five different mixing times of 0.1 s, 0.2 s, 0.3 s, 0.5 s, and 0.7 s using a Bruker Advance NEO 600 MHz NMR Spectrometer associated with a cryo-probe. Since gramicidin A is insoluble in water, we used DMSO-d6 as a solvent. The variation of the intensity of the cross-peaks of the ^{1}H–^{1}H NOESY spectra at five different mixing times was observed and is represented in Table S10 of the SI. The spectrum corresponding to the mixing time of 0.3 s is shown in Fig. 5, and the spectra corresponding to the mixing times of 0.1 s, 0.2 s, 0.5 s, and 0.7 s are shown in Fig. S3 and S4, respectively, in the SI.

Fig. 5 shows the 2D ^{1}H–^{1}H NOESY (nuclear Overhauser effect spectroscopy) spectra of gramicidin A, which provide information about spatial proximity among protons residing on 15 amino acids.[40] The details of the cross-peak assignments and inter-nuclear distances are listed in Tables S9 and S10 of the SI, respectively. This spectrum provides insight into through-space correlations, indicating the structural folding and spatial arrangements within the peptide. In the L-tryptophan (1) residue, the spatial correlations were observed between protons such as H10$_N$–H39, H9$_N$-(H37B, H39), and a network involving H44 with H37A, H37B, and H43. Additionally, H41 shows proximity to H42, while H39 correlates with both H37A and H37B. In the case of L-tryptophan (2), the observed NOE cross-peaks indicate spatial proximity among H13$_N$ and protons H56 and H58, H12$_N$ with H54A, H54B, H53, and H56, as well as correlations among H61 and H54A, H54B, H53, and H60. Further correlations were seen between H58 and H59, H56 with H54A and H53, and H53 with H54A, H54B, and H47. For the L-tryptophan (3) residue, the protons H16$_N$ exhibit spatial proximity with H73 and H75, while H15$_N$ correlates with H71A, H71B, and H73. Protons H78 show NOEs with H71A, H71B, and H77, and additional proximity was observed between H75 and H76, as well as between H73 and H71A and H71B. Similarly, in D-tryptophan (4), spatial interactions were seen among H19$_N$, H90 and H92, and H18$_N$ with H88A, H88B, H81, and H87. Proton H95 shows proximity to H88A, H88B, H87, and H94. Other notable interactions include H92-H93, H87 with H888A, H88B, H82A, and H82B, H88A-H88B and H90 with H88A, H88B, and H87. Moreover, protons H10$_N$, H9$_N$, H39, and H37B in L-tryptophan (1) are spatially connected to several methyl group protons (H35A, H35B, H35C, H34A, H34B, H34C, H23A, H23B,

Table 1 A peak assignment of the 2D ^{1}H–^{15}N HSQC NMR spectrum of gramicidin A

^{15}N isotropic chemical shift (ppm)	^{15}N nuclei	^{1}H isotropic chemical shift (ppm)	Correlated ^{1}H nuclei with ^{15}N nuclei
131.23	N10, N16, N13, N19	10.760	H10$_N$, H16$_N$
		10.705	H13$_N$, H19$_N$
123.80	N9, N1	8.223	H9$_N$, H1$_N$
121.65	N17	8.13	H17$_N$
121.17	N18, N11, N14	8.30	H18$_N$
		8.03	H11$_N$, H14$_N$
120.30	N3, N5	7.99	H3$_N$
		7.92	H5$_N$
120.11	N12, N15	8.20	H12$_N$, H15$_N$
117.50	N4	8.12	H4$_N$
116.07	N7	7.93	H7$_N$
115.68	N8	7.77	H8$_N$
111.93	N6	7.73	H6$_N$
110.20	N20	7.92	H20$_N$
108.75	N2	8.29	H2$_N$

Open Access Article. Published on 10 February 2026. Downloaded on 2/17/2026 2:53:54 PM.
This article is licensed under a Creative Commons Attribution-NonCommercial 3.0 Unported Licence.

H23C), H31 in D-valine (4) and D-valine (2) amino acids. Similarly, methyl protons (H51A, H51B, H51C) and protons H47, H48A, H48B of the D-leucine (2) residue show proximity to protons $H10_N$, $H9_N$, H41, H39, and H37B of L-tryptophan (1). The methyl group of D-valine (4) also shows spatial connections with $H13_N$, $H12_N$, H61, and H56 of L-tryptophan (2).

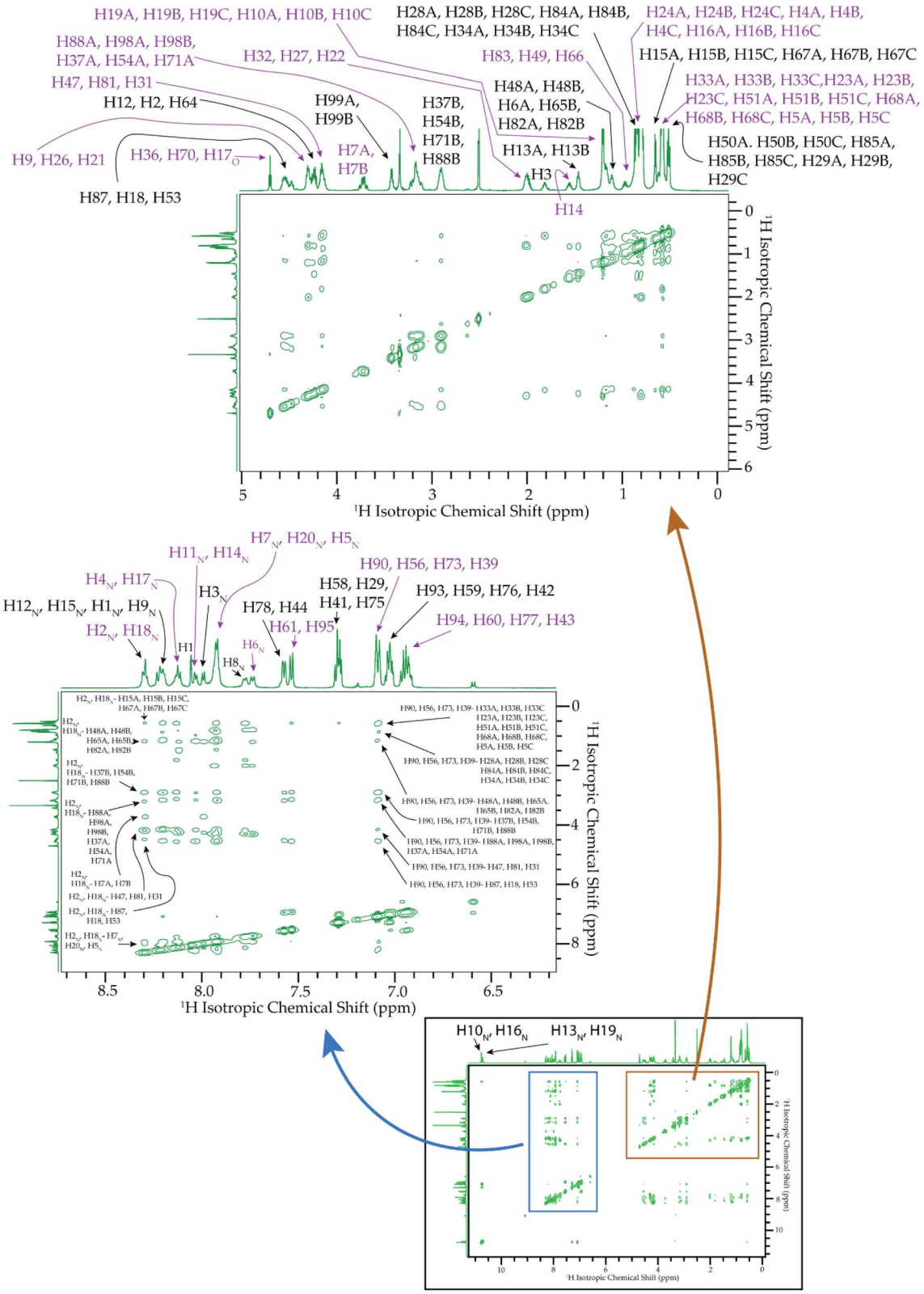

Fig. 5 2D ^{1}H–^{1}H NOESY spectra of gramicidin A.

 © 2026 The Author(s). Published by the Royal Society of Chemistry

Open Access Article. Published on 10 February 2026. Downloaded on 2/17/2026 2:53:54 PM.
This article is licensed under a Creative Commons Attribution-NonCommercial 3.0 Unported Licence.

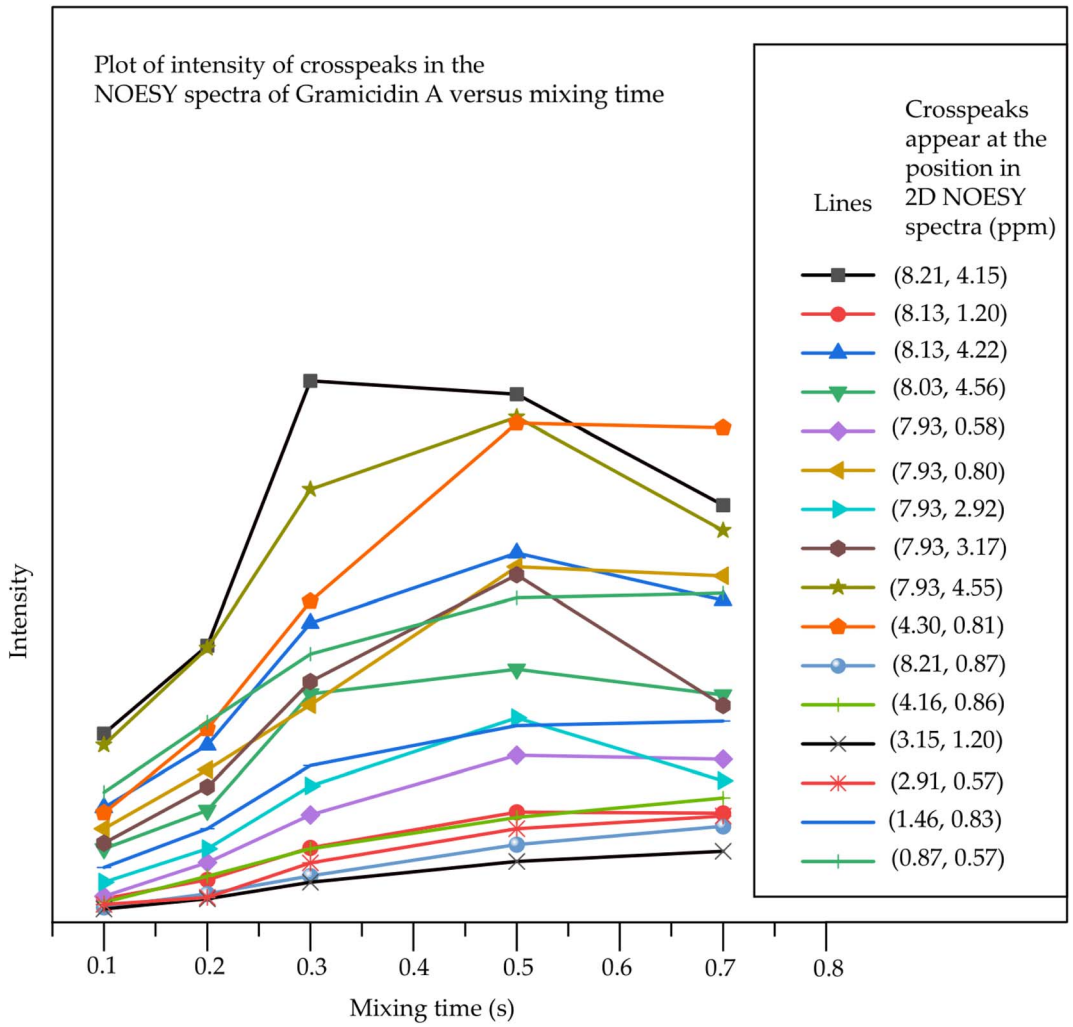

Fig. 6 Plots of NOE intensity with respect to mixing time. The intensity varies nonlinearly after 0.2 s because NOE intensities can be affected by spin diffusion, alternative cross-relaxation pathways, integration uncertainties, variations in local molecular dynamics, structural flexibility, and imperfections in inversion pulses.

Further NOE cross peaks suggest frequent folding of L-tryptophan (2) toward D-leucine (2) and D-leucine (3) residues, as seen from correlations involving $H13_N$, $H12_N$, H61, H58, H56, H54B, and the methyl groups of D-leucine (2) and D-leucine (3). In contrast, minimal NOE contacts between $H15_N$ of L-tryptophan (3) and the methyl protons of D-leucine (2) (H51A, H51B, H51C) suggest limited interaction. However, protons H68A, H68B, H68C, H65A, and H65B of D-leucine (3) show significant proximity to $H16_N$, $H15_N$, H75 and H71B of L-tryptophan (3). The methyl group of D-leucine (4), along with protons H65A and H65B, also showed spatial correlations with D-tryptophan (4).

Additionally, protons bonded to C82 and C84 in D-leucine (4) were found to be spatially close to protons $H18_N$, H88A, H87, and H90 of D-tryptophan (4). Notably, ethanolamine protons also appeared to fold toward D-tryptophan (4), as inferred from correlations with protons $H18_N$, H95, H87, and H88B. In the glycine residue, the $H2_N$ proton showed spatial proximity to $H5_N$ from L-alanine (2) and the methyl protons (H15A, H15B, H15C) of D-leucine (1). Similarly, proton $H4_N$ in L-valine (1) was found to be close to protons H5A, H5B, H5C, H3 and H2 of D-leucine (1). Protons $H6_N$ and H21 in D-valine (2) were in spatial proximity to methyl protons, H22, and H21. Several interactions between D-valine (2) (H23A, H23B, H23C, H24A, H24B, H24C) and D-valine (4) ($H8_N$, H31, H32) indicate a close structural association between these amino acids in gramicidin A. Furthermore, methyl protons H68A, H68B, and H68C in D-leucine (3) showed proximity to protons $H17_N$ and H81 of D-leucine (4). Additional correlations, such as $H11_N$ with H68A, H68B, H68C, H66, and H65A, and the network involving H49, H48, H54A, H54B, H47, H56 with $H14_N$, and H4 with H65A and H65B, suggest a close spatial arrangement between D-leucine (2) and D-leucine (3) amino acids.

Although nuclear Overhauser effects (NOEs) are, in principle, valuable for estimating distances between spatially proximal protons, their quantitative reliability is often limited. NOE intensities can be affected by multiple factors independent of internuclear separation, including spin diffusion, alternative cross-relaxation pathways, integration uncertainties, variations

Open Access Article. Published on 10 February 2026. Downloaded on 2/17/2026 2:53:54 PM.
This article is licensed under a Creative Commons Attribution-NonCommercial 3.0 Unported Licence.

Table 2 Internuclear distances between two protons at a mixing time of 0.1 s

^{1}H isotropic chemical shift (ppm)	^{1}H nuclei	^{1}H isotropic chemical shift of nuclei interacting through NOE (ppm)	^{1}H nuclei interacting through NOE	Internuclear distance calculated from cross peaks in the 2D NOESY spectra (Å)
10.76	$H10_N$, $H16_N$ (protons connected to nitrogens of L-tryptophan (1) and L-tryptophan (3), respectively)	0.57	H33A, H33B, H33C, H23A, H23B, H23C, H51A, H51B, H51C, H68A, H68B, H68C, H5A, H5B, H5C (methyl group protons of D-valine (4), D-valine (2), D-leucine (2), D-leucine (3), and L-valine (1))	2.84
		7.09	H90, H56, H73, H39 (protons connected to carbon C90, C56, C73, and C39 of L-tryptophan groups)	2.09
		7.31	H58, H92, H41, H75 (protons connected to carbon C58, C92, C41, and C75 of indole rings of L-tryptophan groups)	2.65
10.71	$H13_N$, $H19_N$ (protons connected to nitrogens of L-tryptophan (2) and L-tryptophan (4), respectively)	0.57	H33A, H33B, H33C, H23A, H23B, H23C, H51A, H51B, H51C, H68A, H68B, H68C, H5A, H5B, H5C (methyl group protons of D-Valine (4), D-valine (2), D-Leucine (2), D-leucine (3), and L-valine (1))	3.24
		7.09	H90, H56, H73, H39 (protons connected to carbon C90, C56, C73, and C39 of L-tryptophan groups)	2.38
		7.31	H58, H92, H41, H75 (protons connected to carbon C58, C92, C41, and C75 of indole rings of L-tryptophan)	2.98
8.30	$H2_N$, $H18_N$ (protons connected to nitrogen of D-glycine and N18 of L-tryptophan (4), respectively)	0.65	H15A, H15B, H15C, H67A, H67B, H67C (protons connected to methyl groups of D-leucine (1) and D-leucine (3))	3.39
		1.20	H19A, H19B, H19C, H10A, H10B, H10C (protons connected to methyl groups of L-alanine (2) and D-alanine (1))	2.96
		2.91	H37B, H54B, H71B, H88B (protons connected to carbons C37, C54, C71, C88 of L-tryptophan residues)	2.60
		3.23	H98A, H98B, H88A, H37A, H54A, H71A (protons connected to carbon C98 of ethanolamine, C88, C37, C54, C71 of L-tryptophan residues)	3.08
		3.72	H7A, H7B (protons connected to C7 of D-glycine)	2.79
		4.17	H47, H81, H31 (protons connected to C47 of D-leucine (2), C81 of D-leucine (4), C31 of D-valine (4) residues, respectively)	2.22
		4.47	H87, H18, H53 (protons connected to C87 of L-tryptophan (4), C18 of L-alanine (2), C53 of L-tryptophan (2), respectively)	2.98
		7.94	$H7_N$, $H20_N$, $H5_N$ (protons connected to nitrogen of L-valine (3), ethanolamine and L-alanine (2) residues, respectively)	2.77

© 2026 The Author(s). Published by the Royal Society of Chemistry

Open Access Article. Published on 10 February 2026. Downloaded on 2/17/2026 2:53:54 PM.
This article is licensed under a Creative Commons Attribution-NonCommercial 3.0 Unported Licence.

Table 2 (*Contd.*)

^{1}H isotropic chemical shift (ppm)	^{1}H nuclei	^{1}H isotropic chemical shift of nuclei interacting through NOE (ppm)	^{1}H nuclei interacting through NOE	Internuclear distance calculated from cross peaks in the 2D NOESY spectra (Å)
8.21	$H12_N$, $H15_N$, $H1_N$, $H9_N$ (protons connected to nitrogen N12 of L-tryptophan (2), N15 of L-tryptophan (3), N1 of L-valine (1), N1 of L-alanine (2), and N9 of L-tryptophan (1) residues, respectively)	0.58	H33A, H33B, H33C, H23A, H23B, H23C, H51A, H51B, H51C, H68A, H68B, H68C, H5A, H5B, H5C (methyl group protons of D-valine (4), D-valine (2), D-leucine (2), D-leucine (3), and L-valine (1))	2.86
		0.87	H28A, H28B, H28C, H84A, H84B, H84C, H34A, H34B, H34C (protons connected to methyl groups of L-valine (3), D-leucine (4), and D-valine (4) residues)	3.16
		1.11	H48A, H48B, H65A, H65B, H82A, H82B (protons connected to C48 of D-leucine (2), C65 of D-leucine (3), C82 of D-leucine (4))	2.60
		2.91	H37B, H54B, H71B, H88B (protons connected to carbons C37, C54, C71, C88 of L-tryptophan residues)	2.31
		3.17	H98A, H98B, H88A, H37A, H54A, H71A (protons connected to carbon C98 of ethanolamine, C88, C37, C54, C71 of L-tryptophan residues)	2.61
		4.15	H47, H81, H31 (protons connected to C47 of D-leucine (2), C81 of D-leucine (4), C31 of D-valine (4) residues, respectively)	2.08
		4.54	H87, H18, H53 (protons connected to C87 of L-tryptophan (4), L-alanine (2), L-tryptophan (2), respectively)	2.53
		7.09	H90, H56, H73, H39 (protons connected to carbon C90, C56, C73, and C39 of L-tryptophan groups)	3.07
8.13	$H4_N$, $H17_N$ (protons connected to nitrogen N4 of D-leucine (1), and N17 of D-leucine (4) residues, respectively)	0.59	H33A, H33B, H33C, H23A, H23B, H23C, H51A, H51B, H51C, H68A, H68B, H68C, H5A, H5B, H5C (methyl group protons of D-valine (4), D-valine (2), D-leucine (2), D-leucine (3), and L-valine (1))	2.88
		0.83	H28A, H28B, H28C, H84A, H84B, H84C, H34A, H34B, H34C (protons connected to methyl groups of L-valine (3), D-leucine (4), and D-valine (4) residues)	3.27
		1.20	H19A, H19B, H19C, H10A, H10B, H10C (protons connected to the methyl group of L-alanine (2) and D-alanine (1))	2.94
		1.46	H13A, H13B (protons connected to C13 of the D-leucine (1) residue)	2.60
		1.81	H3 (proton connected to C3 of the L-valine (1) residue)	2.87

Open Access Article. Published on 10 February 2026. Downloaded on 2/17/2026 2:53:54 PM.
This article is licensed under a Creative Commons Attribution-NonCommercial 3.0 Unported Licence.

Table 2 (*Contd.*)

^{1}H isotropic chemical shift (ppm)	^{1}H nuclei	^{1}H isotropic chemical shift of nuclei interacting through NOE (ppm)	^{1}H nuclei interacting through NOE	Internuclear distance calculated from cross peaks in the 2D NOESY spectra (Å)
		2.91	H37B, H54B, H71B, H88B (protons connected to carbons C37, C54, C71, C88 of L-tryptophan residues)	2.59
		3.12	H98A, H98B, H88A, H37A, H54A, H71A (protons connected to carbon C98 of ethanolamine, C88, C37, C54, C71 of L-tryptophan residues)	2.96
		4.22	H12, H2, H64 (proton connected to C12 of D-leucine (1), C2 of L-valine (1), C64 of D-leucine (3) residues, respectively)	2.26
		4.56	H87, H18, H53 (protons connected to C87 of L-tryptophan (4), L-alanine (2), L-tryptophan (2), respectively)	2.84
8.03	$H11_N$, $H14_N$ (protons connected to nitrogen N11 of D-leucine (2), and N14 of D-leucine (3) residues)	0.59	H33A, H33B, H33C, H23A, H23B, H23C, H51A, H51B, H51C, H68A, H68B, H68C, H5A, H5B, H5C (methyl group protons of D-valine (4), D-valine (2), D-leucine (2), D-leucine (3), and L-valine (1))	3.63
		0.97	H83, H49, H66 (protons connected to C83 of D-leucine (4), C49 of D-leucine (2), C66 of D-leucine (3) residues, respectively)	3.15
		1.20	H19A, H19B, H19C, H10A, H10B, H10C (protons connected to the methyl groups of L-alanine (2) and D-alanine (1))	2.47
		2.91	H37B, H54B, H71B, H88B (protons connected to carbons C37, C54, C71, C88 of L-tryptophan residues)	3.29
		3.15	H98A, H98B, H88A, H37A, H54A, H71A (protons connected to carbon C98 of ethanolamine, C88, C37, C54, C71 of L-tryptophan residues)	3.14
		4.15	H47, H81, H31 (protons connected to C47 of D-leucine (2), C81 of D-leucine (4), C31 of D-valine (4) residues, respectively)	2.77
		4.56	H87, H18, H53 (protons connected to C87 of L-tryptophan (4), C18 of L-alanine (2), C53 of L-tryptophan (2), respectively)	2.43
7.93	$H7_N$, $H20_N$, $H5_N$ (protons connected to nitrogens of L-valine (3), ethanolamine and L-alanine (2) residues, respectively)	0.58	H33A, H33B, H33C, H23A, H23B, H23C, H51A, H51B, H51C, H68A, H68B, H68C, H5A, H5B, H5C (methyl group protons of D-valine (4), D-valine (2), D-leucine (2), D-leucine (3), and L-valine (1))	2.89

© 2026 The Author(s). Published by the Royal Society of Chemistry

Open Access Article. Published on 10 February 2026. Downloaded on 2/17/2026 2:53:54 PM.
This article is licensed under a Creative Commons Attribution-NonCommercial 3.0 Unported Licence.

Table 2 (*Contd.*)

^{1}H isotropic chemical shift (ppm)	^{1}H nuclei	^{1}H isotropic chemical shift of nuclei interacting through NOE (ppm)	^{1}H nuclei interacting through NOE	Internuclear distance calculated from cross peaks in the 2D NOESY spectra (Å)
		0.80	H24A, H24B, H24C, H4A, H4B, H4C, H16A, H16B, H16C (protons connected to one of the methyl groups of D-valine (2), L-valine (1), and D-leucine (1) residues)	2.34
		1.20	H19A, H19B, H19C, H10A, H10B, H10C (protons connected to the methyl groups of L-alanine (2) and D-alanine (1) residues)	2.13
		1.46	H13A, H13B (protons connected to C13 of D-leucine (1) residue)	3.36
		2.01	H32, H27, H22 (protons connected to C32 of D-valine (4), L-valine (3), and D-valine (2))	2.55
		2.92	H37B, H54B, H71B, H88B (protons connected to carbons C37, C54, C71, C88 of L-tryptophan residues)	2.69
		3.17	H98A, H98B, H88A, H37A, H54A, H71A (protons connected to carbon C98 of ethanolamine, C88, C37, C54, C71 of L-tryptophan residues)	2.40
		4.29	H9, H26, H21 (protons connected to C9 of L-alanine (1), C26 of L-valine (3), and C21 of *S*-valine (2) residues)	2.13
		4.55	H87, H18, H53 (protons connected to C87 of L-tryptophan (4), L-alanine (2), L-tryptophan (2), respectively)	2.10
		7.77	$H8_N$ (proton connected to nitrogen N8 of the L-valine (3) residue)	2.49
		7.74	$H6_N$ (proton connected to nitrogen N8 of the D-valine (2) residue)	2.44
7.78	$H8_N$ (proton connected to nitrogen N8 of the L-valine (3) residue)	0.59	H33A, H33B, H33C, H23A, H23B, H23C, H51A, H51B, H51C, H68A, H68B, H68C, H5A, H5B, H5C (methyl group protons of D-valine (4), D-valine (2), D-leucine (2), D-leucine (3), and L-valine (1))	2.54
		0.78	H24A, H24B, H24C, H4A, H4B, H4C, H16A, H16B, H16C (protons connected to one of the methyl groups of D-valine (2), L-valine (1), and D-leucine (1) residues)	2.85
		1.81	H3 (proton connected to C3 of the L-valine (1) residue)	2.93
		2.01	H32, H27, H22 (protons connected to C32 of D-valine (4), L-valine (3), and D-valine (2))	2.82
		4.29	H9, H26, H21 (protons connected to C9 of L-alanine (1), C26 of L-valine (3), and C21 of *S*-valine (2) residues)	2.30

© 2026 The Author(s). Published by the Royal Society of Chemistry

Open Access Article. Published on 10 February 2026. Downloaded on 2/17/2026 2:53:54 PM.
This article is licensed under a Creative Commons Attribution-NonCommercial 3.0 Unported Licence.

Table 2 (*Contd.*)

^{1}H isotropic chemical shift (ppm)	^{1}H nuclei	^{1}H isotropic chemical shift of nuclei interacting through NOE (ppm)	^{1}H nuclei interacting through NOE	Internuclear distance calculated from cross peaks in the 2D NOESY spectra (Å)
7.73	$H6_N$ (proton connected to nitrogen N8 of the D-valine (2) residue)	0.80	H24A, H24B, H24C, H4A, H4B, H4C, H16A, H16B, H16C (protons connected to one of the methyl groups of D-valine (2), L-valine (1), and D-leucine (2) residues)	2.54
		1.20	H19A, H19B, H19C, H10A, H10B, H10C (protons connected to the methyl groups of L-alanine (2) and D-alanine (1))	2.82
		2.01	H32, H27, H22 (protons connected to C32 of D-valine (4), L-valine (3), and D-valine (2))	2.92
		4.31	H9, H26, H21 (protons connected to C9 of L-alanine (1), C26 of L-valine (3), and C21 of D-valine (2) residues)	2.25
7.57	H78, H44 (protons connected to C78 of L-tryptophan (3) and C44 of L-tryptophan (1) residues	2.91	H37B, H54B, H71B, H88B (protons connected to carbons C37, C54, C71, C88 of L-tryptophan residues)	3.30
		3.18	H98A, H98B, H88A, H37A, H54A, H71A (protons connected to carbon C98 of ethanolamine, C88, C37, C54, C71 of L-tryptophan residues)	3.06
		4.53	H87, H18, H53 (protons connected to C87 of L-tryptophan (4), L-alanine (2), L-tryptophan (2) respectively)	2.87
		6.95	H94, H60, H77, H43 (protons connected to C94, C60, C77, C43 of benzene rings in L-tryptophan residues)	2.86
7.54	H61, H95 (protons connected to C61 of L-tryptophan (2) and C95 of L-tryptophan (4) residues	0.57	H33A, H33B, H33C, H23A, H23B, H23C, H51A, H51B, H51C, H68A, H68B, H68C, H5A, H5B, H5C (methyl group protons of D-valine (4), D-valine (2), D-leucine (2), D-leucine (3), and L-valine (1))	3.19
		2.91	H37B, H54B, H71B, H88B (protons connected to carbons C37, C54, C71, C88 of L-tryptophan residues)	2.89
		3.14	H98A, H98B, H88A, H37A, H54A, H71A (protons connected to carbon C98 of ethanolamine, C88, C37, C54, C71 of L-tryptophan residues)	2.75
		4.51	H87, H18, H53 (protons connected to C87 of L-tryptophan (4), L-alanine (2), L-tryptophan (2), respectively)	2.68
		6.95	H94, H60, H77, H43 (protons connected to C94, C60, C77, C43 of benzene rings in L-tryptophan residues respectively)	2.37
7.29		0.57		3.21

© 2026 The Author(s). Published by the Royal Society of Chemistry

Open Access Article. Published on 10 February 2026. Downloaded on 2/17/2026 2:53:54 PM.
This article is licensed under a Creative Commons Attribution-NonCommercial 3.0 Unported Licence.

Table 2 (*Contd.*)

^{1}H isotropic chemical shift (ppm)	^{1}H nuclei	^{1}H isotropic chemical shift of nuclei interacting through NOE (ppm)	^{1}H nuclei interacting through NOE	Internuclear distance calculated from cross peaks in the 2D NOESY spectra (Å)
	H58, H92, H41, H75 (protons connected to C58, C92, C41, C75 of indole rings in L-tryptophan residues)		H33A, H33B, H33C, H23A, H23B, H23C, H51A, H51B, H51C, H68A, H68B, H68C, H5A, H5B, H5C (methyl group protons of D-valine (4), D-valine (2), D-leucine (2), D-leucine (3), and L-valine (1))	
		7.03	H93, H59, H76, H42 (protons connected to C93, C59, C76, C42 of benzene rings in L-tryptophan residues)	2.41
7.08	H90, H56, H73, H39 (protons connected to C90, C56, C73, C39 of L-tryptophan residues)	0.57	H33A, H33B, H33C, H23A, H23B, H23C, H51A, H51B, H51C, H68A, H68B, H68C, H5A, H5B, H5C (methyl group protons of D-valine (4), D-valine (2), D-leucine (2), D-leucine (3), and L-valine (1))	2.66
		0.85	H28A, H28B, H28C, H84A, H84B, H84C, H34A, H34B, H34C (protons connected to methyl groups of L-valine (3), D-leucine (4), and D-valine (4) residues)	3.22
		1.20	H19A, H19B, H19C, H10A, H10B, H10C (protons connected to the methyl groups of L-alanine (2) and D-alanine (1))	3.04
		2.91	H37B, H54B, H71B, H88B (protons connected to carbons C37, C54, C71, C88 of L-tryptophan residues)	2.47
		3.17	H98A, H98B, H88A, H37A, H54A, H71A (protons connected to carbon C98 of ethanolamine, C88, C37, C54, C71 of L-tryptophan residues)	2.78
		4.15	H47, H81, H31 (protons connected to C47 of D-leucine (2), C81 of D-leucine (4), C31 of D-valine (4) residues, respectively)	3.32
		4.54	H87, H18, H53 (protons connected to C87 of L-tryptophan (4), L-alanine (2), L-tryptophan (2), respectively)	2.81
4.54	H87, H18, H53 (protons connected to C87 of L-tryptophan (4), L-alanine (2), L-tryptophan (2), respectively)	1.20	H19A, H19B, H19C, H10A, H10B, H10C (protons connected to the methyl groups of L-alanine (2) and D-alanine (1))	3.23
		2.91	H37B, H54B, H71B, H88B (protons connected to carbons C37, C54, C71, C88 of L-tryptophan residues)	2.44
		3.16	H98A, H98B, H88A, H37A, H54A, H71A (protons connected to carbon C98 of ethanolamine, C88, C37, C54, C71 of L-tryptophan residues)	2.49
		4.15		3.16

Open Access Article. Published on 10 February 2026. Downloaded on 2/17/2026 2:53:54 PM.
This article is licensed under a Creative Commons Attribution-NonCommercial 3.0 Unported Licence.

Table 2 (*Contd.*)

^{1}H isotropic chemical shift (ppm)	^{1}H nuclei	^{1}H isotropic chemical shift of nuclei interacting through NOE (ppm)	^{1}H nuclei interacting through NOE	Internuclear distance calculated from cross peaks in the 2D NOESY spectra (Å)
			H47, H81, H31 (protons connected to C47 of D-leucine (2), C81 of D-leucine (4), C31 of D-valine (4) residues, respectively)	
4.30	H9, H26, H21 (protons connected to C9 of L-alanine (1), C26 of L-valine (3), and C21 of *S*-valine (2) residues)	0.57	H33A, H33B, H33C, H23A, H23B, H23C, H51A, H51B, H51C, H68A, H68B, H68C, H5A, H5B, H5C (methyl group protons of D-valine (4), D-valine (2), D-leucine (2), D-leucine (3), and L-valine (1))	3.22
		0.81	H24A, H24B, H24C, H4A, H4B, H4C, H16A, H16B, H16C (protons connected to one of the methyl groups of D-valine (2), L-valine (1), and D-leucine (1) residues)	2.28
		1.20	H19A, H19B, H19C, H10A, H10B, H10C (protons connected to the methyl groups of L-alanine (2) and D-alanine (1))	2.52
		2.02	H32, H27, H22 (protons connected to C32 of D-valine (4), L-valine (3), and D-valine (2))	2.44
4.24	H12, H2, H64 (protons connected to C12 of D-leucine (1), C2 of L-valine (1), C64 of D-leucine (3) residues, respectively)	0.79	H24A, H24B, H24C, H4A, H4B, H4C, H16A, H16B, H16C (protons connected to one of the methyl groups of D-valine (2), L-valine (1), and D-leucine (1) residues)	2.73
		1.46	H13A, H13B (protons connected to C13 of D-leucine (1) residue)	2.56
4.16	H47, H81, H31 (protons connected to C47 of D-leucine (2), C81 of D-leucine (4), C31 of D-valine (4) residues, respectively)	0.58	H33A, H33B, H33C, H23A, H23B, H23C, H51A, H51B, H51C, H68A, H68B, H68C, H5A, H5B, H5C (methyl group protons of D-valine (4), D-valine (2), D-leucine (2), D-leucine (3), and L-valine (1))	2.18
		0.86	H28A, H28B, H28C, H84A, H84B, H84C, H34A, H34B, H34C (protons connected to methyl groups of L-valine (3), D-leucine (4), and D-valine (4) residues)	3.02
		1.20	H19A, H19B, H19C, H10A, H10B, H10C (protons connected to the methyl groups of L-alanine (2) and D-alanine (1))	2.28
		1.81	H3 (proton connected to C3 of L-valine (1) residue)	2.71
		2.91	H37B, H54B, H71B, H88B (protons connected to carbons C37, C54, C71, C88 of L-tryptophan residues)	3.14
3.15	H98A, H98B, H88A, H37A, H54A, H71A (protons connected to carbon C98 of ethanolamine, C88,	0.57	H33A, H33B, H33C, H23A, H23B, H23C, H51A, H51B, H51C, H68A, H68B, H68C, H5A, H5B, H5C (methyl group protons of	3.32

© 2026 The Author(s). Published by the Royal Society of Chemistry

Open Access Article. Published on 10 February 2026. Downloaded on 2/17/2026 2:53:54 PM.
This article is licensed under a Creative Commons Attribution-NonCommercial 3.0 Unported Licence.

Table 2 (*Contd.*)

^{1}H isotropic chemical shift (ppm)	^{1}H nuclei	^{1}H isotropic chemical shift of nuclei interacting through NOE (ppm)	^{1}H nuclei interacting through NOE	Internuclear distance calculated from cross peaks in the 2D NOESY spectra (Å)
	C37, C54, C71 of L-tryptophan residues)		D-valine (4), D-valine (2), D-leucine (2), D-leucine (3), and L-valine (1))	
		1.20	H19A, H19B, H19C, H10A, H10B, H10C (protons connected to the methyl groups of L-alanine (2) and D-alanine (1))	3.22
		2.91	H37B, H54B, H71B, H88B (protons connected to carbons C37, C54, C71, C88 of L-tryptophan residues)	1.74
2.91	H37B, H54B, H71B, H88B (protons connected to carbons C37, C54, C71, C88 of L-tryptophan residues)	0.57	H33A, H33B, H33C, H23A, H23B, H23C, H51A, H51B, H51C, H68A, H68B, H68C, H5A, H5B, H5C (methyl group protons of D-valine (4), D-valine (2), D-leucine (2), D-leucine (3), and L-valine (1))	3.07
		1.20	H19A, H19B, H19C, H10A, H10B, H10C (protons connected to the methyl groups of L-alanine (2) and D-alanine (1))	3.08
2.01	H32, H27, H22 (protons connected to C32 of D-valine (4), L-valine (3), and D-valine (2))	0.81	H24A, H24B, H24C, H4A, H4B, H4C, H16A, H16B, H16C (protons connected to one of the methyl groups of D-valine (2), L-valine (1), and D-leucine (1) residues)	2.08
1.81	H3 (proton connected to C3 of L-valine (1) residue)	0.57	H33A, H33B, H33C, H23A, H23B, H23C, H51A, H51B, H51C, H68A, H68B, H68C, H5A, H5B, H5C (methyl group protons of D-valine (4), D-valine (2), D-leucine (2), D-leucine (3), and L-valine (1))	2.41
1.56	H14 (proton connected to C14 of the D-leucine (1) residue)	0.83	H28A, H28B, H28C, H84A, H84B, H84C, H34A, H34B, H34C (protons connected to methyl groups of L-valine (3), D-leucine (4), and D-valine (4) residues)	2.73
1.46	H13A, H13B (protons connected to C13 of the D-leucine (1) residue)	0.83	H28A, H28B, H28C, H84A, H84B, H84C, H34A, H34B, H34C (protons connected to methyl groups of L-valine (3), D-leucine (4), and D-valine (4) residues)	2.55
1.20	H19A, H19B, H19C, H10A, H10B, H10C (protons connected to the methyl groups of L-alanine (2) and D-alanine (1))	0.57	H33A, H33B, H33C, H23A, H23B, H23C, H51A, H51B, H51C, H68A, H68B, H68C, H5A, H5B, H5C (methyl group protons of D-valine (4), D-valine (2), D-leucine (2), D-leucine (3), and L-valine (1))	2.29
0.87	H28A, H28B, H28C, H84A, H84B, H84C, H34A, H34B, H34C (protons connected to methyl groups of L-valine (3), D-leucine (4), and D-valine (4) residues)	0.57	H33A, H33B, H33C, H23A, H23B, H23C, H51A, H51B, H51C, H68A, H68B, H68C, H5A, H5B, H5C (methyl group protons of D-valine (4), D-valine (2), D-leucine (2), D-leucine (3), and L-valine (1))	2.21

© 2026 The Author(s). Published by the Royal Society of Chemistry

Open Access Article. Published on 10 February 2026. Downloaded on 2/17/2026 2:53:54 PM.
This article is licensed under a Creative Commons Attribution-NonCommercial 3.0 Unported Licence.

in local molecular dynamics, structural flexibility, and imperfections in inversion pulses.[41–44] These contributions become increasingly dominant at longer mixing times. However, under the initial-rate approximation, the NOE intensity is approximately proportional to the product of the mixing time (τ_m) and the cross-relaxation rate (σ):[41–44]

$$I = \sigma\ \tau_m \tag{1}$$

The cross-relaxation rate can be expressed by the following equation:

$$\sigma = kr^{-6} \tag{2}$$

where k is a constant represented by the equation

$$k = \left(\frac{\mu_0}{4\pi}\right)^2 \frac{\hbar^2\gamma^2}{10}\left(\frac{6\tau_c}{1+4\omega^2\tau_c{}^2} - \tau_c\right)$$

where μ_0, γ, and ω are the magnetic permeability in free space, the gyromagnetic ratio of the proton, and the Larmor frequency of the proton, respectively, and the correlation time τ_c is assumed to be nearly the same for all the proton pairs.

Therefore, overall, the intensity is proportional to the mixing time and r^{-6} at the short mixing time,[41,42]

$$I \propto \tau_m r^{-6} \tag{3}$$

The variation of the NOE intensity with different mixing times (0.1 s, 0.2 s, 0.3 s, 0.5 s, and 0.7 s) for different spatially close protons in gramicidin A is given in Table S10 of the SI, and the plot of the NOE intensity *versus* mixing time is shown in Fig. 6. For gramicidin A, the NOE intensities increase non-linearly after 0.2 s due to different perturbations, except for internuclear distance, as discussed earlier.

Therefore, the internuclear distance between the spatially closed protons was determined at a small mixing time (*i.e.*, 0.1 s) to avoid inaccuracy. The ratio of intensities (I and I_{ref}) of two cross peaks in the NOESY spectra is proportional to the ratio of the internuclear distance between the spatially close protons (r and r_{ref}) raised to the power of −6.[41]

$$\frac{I}{I_{ref}} = \left(\frac{r_{ref}}{r}\right)^6 \tag{4}$$

Here, I represents the intensity of cross peaks in the 2D NOESY spectra corresponding to nuclei whose internuclear distances are unknown, and I_{ref} indicates the intensity of cross peaks corresponding to nuclei with known internuclear distances. Here, *ortho*-positioned protons, such as (H58, H59), (H92, H93), (H41, H42), and (H75, H76), in the benzene ring of tryptophan residues are taken as references (*i.e.*, $I_{ref} = 6.252 \times 10^9$ and $r_{ref} =$ 2.41 Å). The calculated internuclear distances at the mixing time of 0.1 s are reported in Table 2. The distances were found to range from 2.08 Å to 3.70 Å.

Determining proton–proton internuclear distances (r) is essential for understanding the structure and function of peptide systems, as these distances provide direct insight into the three-dimensional folding of the peptide backbone. The resulting folding–unfolding behaviour has a pronounced influence on biological activity.[42–44] As summarized in Table 2, the internuclear distance between the indole N–H proton of the five-membered pyrrole ring in the side chain of L-tryptophan (1) and L-tryptophan (3) and the methyl protons of L-valine (1), D-valine (2), D-valine (4), D-leucine (2), and D-leucine (3) is 2.84 Å. Likewise, the corresponding internuclear distance for the indole N–H proton of L-tryptophan (2) and L-tryptophan (4) relative to the same set of methyl groups is 3.23 Å. The internuclear distances between the protons of the methyl groups of D-leucine (1) and D-leucine (3) and protons of the methyl groups of D-alanine (1) and L-alanine (2), and the protons connected to the nitrogen atoms of D-glycine and L-tryptophan(4) are 3.39 Å and 2.96 Å.

These values indicate the spatial proximity between these amino-acid residues and the proteinogenic amino acid tryptophan, which contains two aromatic rings and displays unique physicochemical properties due to the presence of an indole ring, containing a hydrophobic benzene ring and a hydrophilic N–H bond in the pyrrole ring. The positional isomerism of the tryptophan residue controls the overall hydrophobicity and biological activity of the polypeptide antibiotic. The spatial proximity of other amino acids, like L-valine (1), D-valine (2), D-valine (4), D-leucine (1), D-leucine (2), D-leucine (3), D-alanine (1), and L-alanine (2), as revealed by the NOESY experiment, is very crucial for understanding the role of the tryptophan residue in the physicochemical properties of gramicidin A.

3.3 Analysis of ^{13}C CP-MAS SSNMR spectra and determination of the principal components of the chemical shift anisotropy (CSA) tensor by the ^{13}C 2DPASS CP-MAS SSNMR experiment

The combined XRD and NMR crystallography approach provides a more complete and accurate understanding of the structure and dynamics of solids, enabling the identification of subtle local distortions, disorder, or conformational variations that are often averaged out in diffraction data.[41]

Fig. 7 shows the ^{13}C CP-MAS SSNMR spectrum of gramicidin A. The spinning CSA sideband patterns for the chemically distinct ^{13}C nuclei are shown in Fig. 9, while Fig. 8 presents the ^{13}C 2D PASS CP-MAS solid-state NMR spectrum of gramicidin A. In a 2D PASS experiment, the isotropic and anisotropic chemical shifts are resolved along two orthogonal axes. As illustrated in Fig. 9, carbon sites experiencing different local chemical environments are dispersed along the horizontal axis according to their characteristic isotropic chemical shifts. In contrast, the number and relative intensities of the spinning sidebands distributed along the vertical axis report directly on the magnitude of the chemical shift anisotropy (CSA).[45–51] Because the sidebands appear at multiples of the MAS frequency, relatively slow spinning rates of 500 Hz and 2 kHz were employed to ensure adequate observation of CSA patterns for both aromatic and aliphatic carbon sites.

The isotropic chemical shift values (as presented in Table S11 of the SI) and the principal components of the chemical shift anisotropy (CSA) tensor (Table 3) for carbonyl group carbon nuclei in five distinct amino acid residues of gramicidin A were observed to be the highest among all carbon nuclei sites.

 © 2026 The Author(s). Published by the Royal Society of Chemistry

Open Access Article. Published on 10 February 2026. Downloaded on 2/17/2026 2:53:54 PM.
This article is licensed under a Creative Commons Attribution-NonCommercial 3.0 Unported Licence.

This pronounced chemical shift behavior can be attributed to several interrelated structural and electronic factors. A primary contributing factor is the presence of hydrogen bonding between peptide backbone units. Specifically, the carbonyl oxygen of one amino acid residue forms a hydrogen bond with the amide hydrogen of an adjacent residue. This interaction gives rise to a continuous and well-organized hydrogen-bonding network along the helical backbone of gramicidin A. Such a network not only imparts significant structural stability to the helix but also plays a vital role in maintaining the integrity of the ion-conducting channel, facilitating selective ion transport across the membrane. These hydrogen bonds substantially influence the electronic environment of the carbonyl carbon. By pulling electron density toward the oxygen atom, they induce polarization within the carbonyl group, thereby altering the distribution of the surrounding electron cloud. This polarization effect enhances the deshielding of the carbon nucleus, leading to a higher chemical shift value. Additionally, the inherently polar nature of the carbonyl group, which involves a double bond between carbon and a highly electronegative oxygen, contributes to a strong electrostatic effect. The uneven distribution of electron density across this polar bond further shifts the chemical shift values to higher frequencies.

Another important factor responsible for the large CSA values is magnetic anisotropy, which arises from the lack of symmetry in the carbonyl group. Unlike methyl or methylene groups, the carbonyl moiety lacks symmetrical geometry, resulting in direction-dependent magnetic susceptibility. In other words, the carbonyl group exhibits different responses to the magnetic field along the three principal axes. This asymmetry leads to two distinct anisotropic susceptibilities, one aligned parallel and the other perpendicular to the external magnetic field. The directional variation in magnetic shielding caused by this anisotropy generates a large value of CSA parameters. Hence, the higher values of the isotropic and anisotropic chemical shifts of carbonyl carbons in gramicidin A are a combined consequence of hydrogen bonding, a polar bond with an uneven charge distribution, and magnetic anisotropy. These factors collectively underscore the unique chemical environment experienced by the carbonyl carbons, reflecting their crucial role in the structural and functional architecture of the peptide.

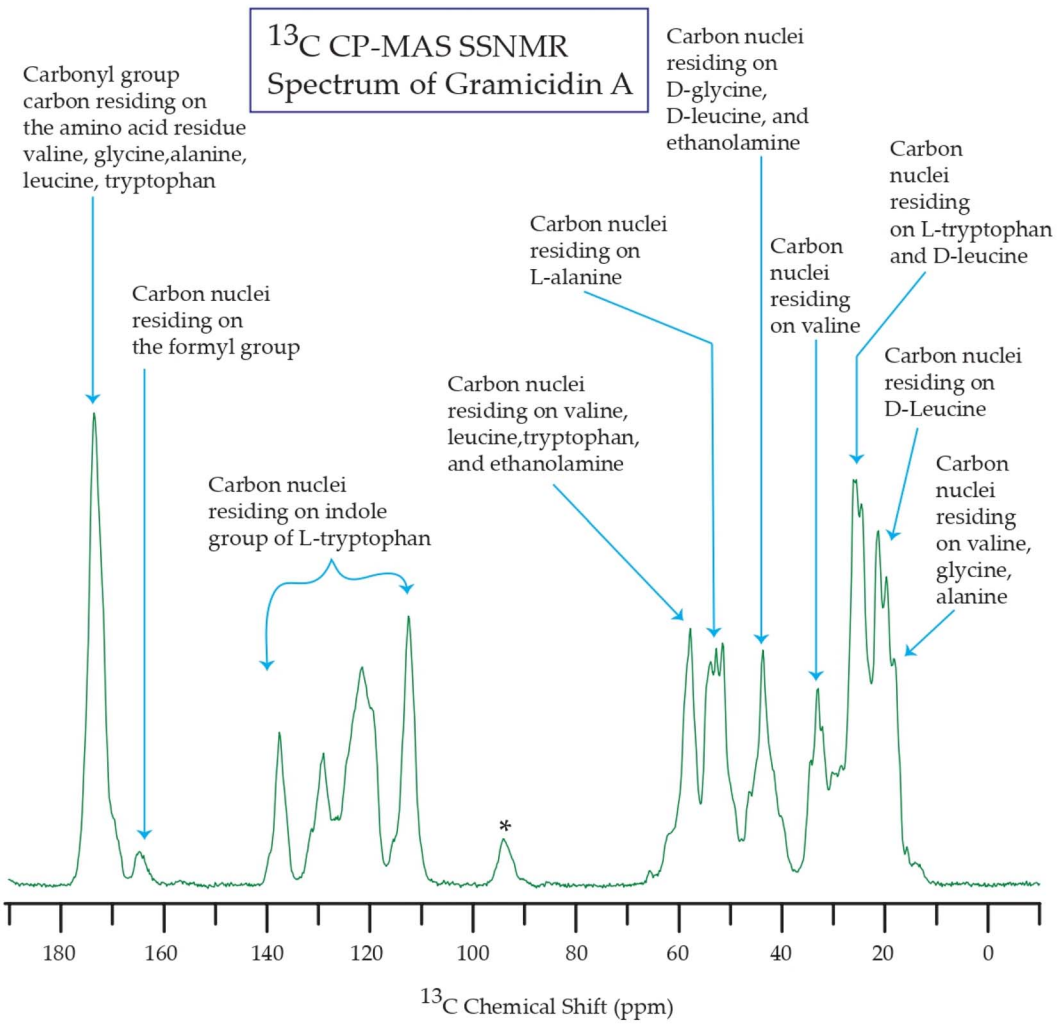

Fig. 7 ^{13}C CP-MAS SSNMR spectrum of gramicidin A.

Open Access Article. Published on 10 February 2026. Downloaded on 2/17/2026 2:53:54 PM.
This article is licensed under a Creative Commons Attribution-NonCommercial 3.0 Unported Licence.

The resonance lines from 137.8 ppm to 112.6 ppm correspond to different carbon nuclei in the amino acid tryptophan. Tryptophan residues are essential for stabilizing the structures of channels. Their hydrogen bonds help to maintain the single-stranded, head-to-head dimeric conformation of the channel. Table 3 reveals that the 'span' of the chemical shift anisotropy (CSA) sideband pattern for the carbon nuclei located on the indole ring of the L-tryptophan residue is the highest among all the carbon sites in this linear peptide antibiotic. This can be attributed to the presence of the aromatic side chain in tryptophan, which significantly influences its electronic environment. The higher CSA values observed for these carbon nuclei stem from the delocalized π-electrons in the aromatic ring. When these π-electrons circulate in a clockwise direction under the influence of the external magnetic field, they induce a secondary magnetic field that aligns with the applied field. This phenomenon increases the overall magnetic field experienced by the nucleus, resulting in what is known as the deshielding effect. Conversely, when the π-electrons circulate in an anticlockwise direction, the induced magnetic field opposes the external field, thereby reducing the effective magnetic field experienced by the nucleus—a phenomenon termed the shielding effect. These magnetic shielding and deshielding interactions contribute to the large CSA parameters typically observed for carbon nuclei within aromatic systems, particularly those surrounded by nonbonded electron clouds. The presence of the aromatic indole side chain plays a vital role in the biological function of the peptide. Tryptophan residues are known to engage in strong interactions with bacterial membranes due to their amphipathic and aromatic nature. These interactions can lead to membrane destabilization, facilitating the anchoring of antimicrobial peptides (AMPs) to the lipid bilayer and promoting membrane disruption. Through these mechanisms, tryptophan residues are crucial contributors to the antimicrobial efficacy of AMPs. Hence, the higher values of the CSA parameters for the aromatic amino acid residue like tryptophan is experimental evidence of the involvement of this amino acid with intermolecular and intramolecular hydrogen bonds, because there induced a polarization on the electron-cloud due to hydrogen bond and electrostatic interaction is also enhanced. The ^{13}C spin-lattice relaxation mechanism is dominated by the CSA-interactions and heteronuclear dipole–dipole interactions, and for non-protonated carbon nuclei, only the CSA interaction plays a key role at high values of the magnetic field. In a subsequent section, we will observe that the spin-lattice relaxation times and the local correlation times are longer for those carbon nuclei residing on the indole group of L-tryptophan. This is also experimental evidence that the aromatic cluster is formed due to π–π stacking interactions (spin-lattice relaxation time is longer due to the π–π stacking interactions), which play a key role in the mechanism of membrane binding and interaction.[23,24]

3.4 ^{1}H–^{13}C heteronuclear correlation (HETCOR) SSNMR spectrum of gramicidin A

Molecular dynamics play a crucial role in modulating the dipolar coupling between ^{1}H and ^{13}C nuclei, which can be effectively probed through a two-dimensional ^{1}H–^{13}C HETCOR (heteronuclear correlation) experiment. To enhance resolution

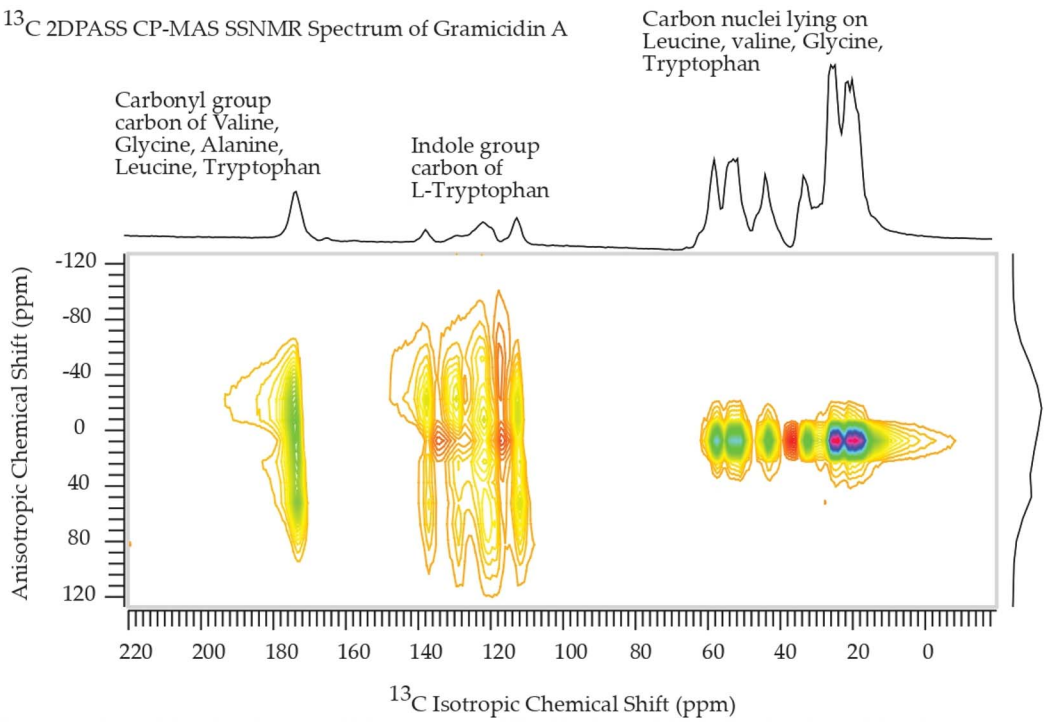

Fig. 8 ^{13}C 2DPASS CP-MAS SSNMR spectrum of gramicidin A. The direct dimension represents a purely isotropic spectrum with infinite spinning frequency. The number and the intensity of the spinning sidebands can be extracted from the indirect dimension, which are related to the chemical shift anisotropy of the individual carbon sites.

 © 2026 The Author(s). Published by the Royal Society of Chemistry

Open Access Article. Published on 10 February 2026. Downloaded on 2/17/2026 2:53:54 PM.
This article is licensed under a Creative Commons Attribution-NonCommercial 3.0 Unported Licence.

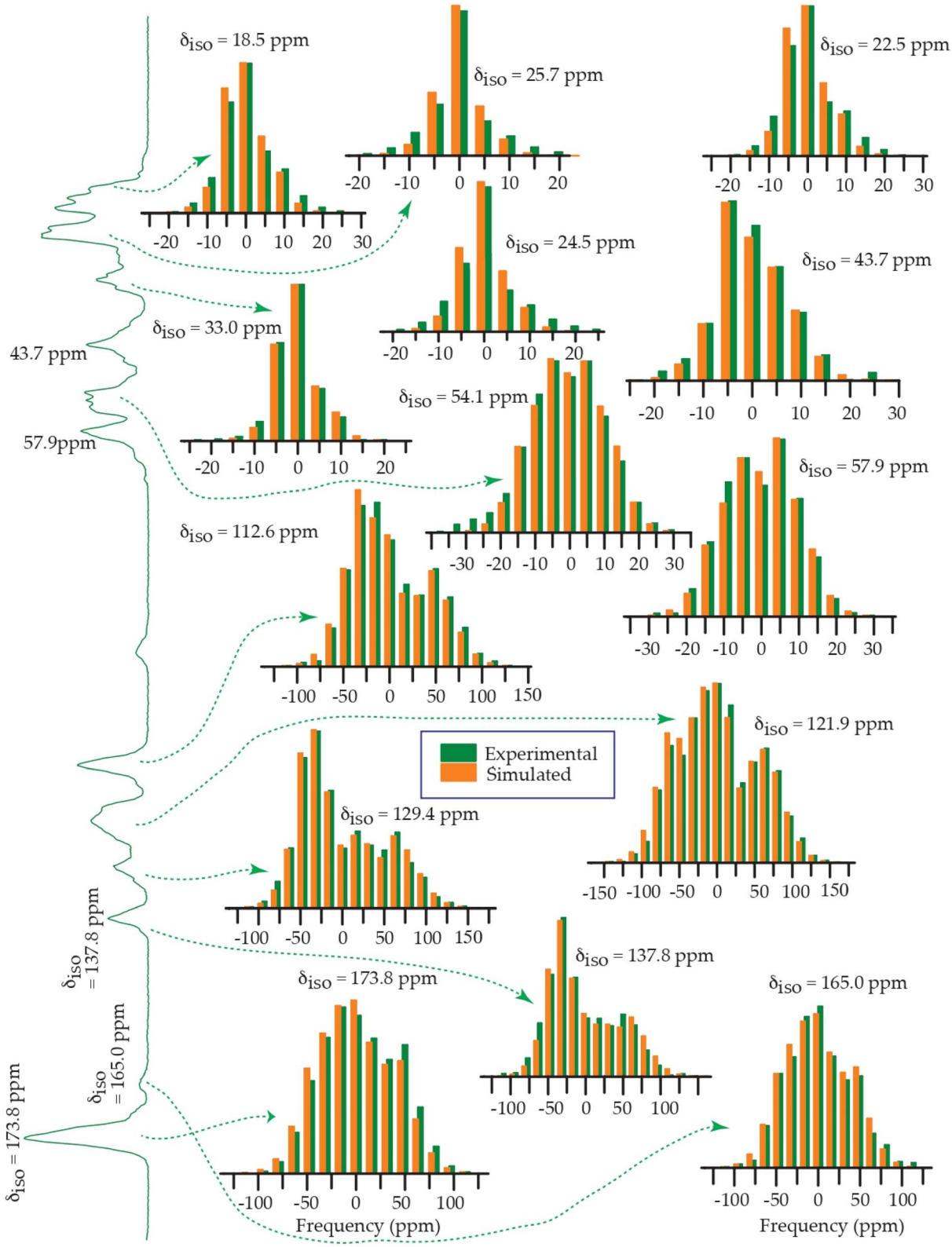

Fig. 9 The spinning CSA sideband pattern of various carbon nuclei residing on gramicidin A.

Open Access Article. Published on 10 February 2026. Downloaded on 2/17/2026 2:53:54 PM.
This article is licensed under a Creative Commons Attribution-NonCommercial 3.0 Unported Licence.

Table 3 ^{13}C chemical shift anisotropy (CSA) parameters of gramicidin A[a]

Carbon nuclei	δ_{iso}(ppm)	δ_{11}(ppm)	δ_{22}(ppm)	δ_{33}(ppm)	Span (ppm)	Skew	Anisotropy ($\Delta\delta$) (ppm)	Asymmetry(η)
Carbonyl group carbons of valine, glycine, alanine, leucine, tryptophan	173.8	249.9 ± 0.6	168.3 ± 0.5	103.0 ± 0.4	146.9 ± 0.7	−0.1	114.2 ± 1.0	0.8
Carbon nuclei of the formyl group	165.0	241.7 ± 1.3	159.7 ± 1.9	93.6 ± 1.8	148.1 ± 1.9	−0.1	115.0 ± 1.7	0.8
Carbon nuclei residing on the indole group of L-tryptophan	137.8	241.4 ± 1.4	101.2 ± 1.1	70.7 ± 0.8	170.7 ± 1.2	−0.6	155.5 ± 2.1	0.3
Carbon nuclei residing on the indole group of L-tryptophan	129.4	240.3 ± 1.3	89.6 ± 1.1	58.3 ± 0.8	181.9 ± 1.1	−0.6	166.3 ± 2.0	0.3
Carbon nuclei residing on the indole group of L-tryptophan	121.9	230.7 ± 1.2	109.9 ± 1.9	25.0 ± 1.3	205.7 ± 1.7	−0.2	163.2 ± 1.3	0.8
Carbon nuclei residing on the indole group of L-tryptophan	112.6	201.8 ± 1.8	91.8 ± 1.2	44.2 ± 1.1	157.5 ± 1.3	−0.4	133.7 ± 2.7	0.5
C2-L-valine C12-D-leucine C21-D-valine C26-L-valine C31-D-valine C36-L-tryptophan C47-D-leucine C53-L-tryptophan C64 -D-leucine C70-L-tryptophan C81- D-leucine C87-L-tryptophan C99-carbon nuclei residing on the molecular moiety ethanolamine ($NHCH_2CH_2OH$)	57.9	75.9 ± 0.1	58.5 ± 0.1	39.2 ± 0.1	36.7 ± 0.2	0	−28.0 ± 0.2	0.9
C9, C18	54.1	73.5 ± 0.2	54.0 ± 0.1	34.7 ± 0.1	38.8 ± 0.2	0	29.1 ± 0.3	1.0
C7-D-glycine (D-gly) C13-D-leucine (D-leu) C48-D-leucine (D-leu) C65-D-leucine (D-leu) C82-D-leucine (D-leu) C98 residing on the residue of ethanolamine	43.7	58.3 ± 0.2	41.4 ± 0.1	31.3 ± 0.2	27.0 ± 0.4	−0.2	21.9 ± 0.4	0.7
C22- D-valine C27-L-valine C32-D-valine	33.0	44.0 ± 0.06	29.8 ± 0.04	25.1 ± 0.04	18.9 ± 0.07	−0.5	16.5 ± 0.09	0.4
C37-L-tryptophan C54-L-tryptophan C88-L-tryptophan C71-L-tryptophan	25.7	35.1 ± 0.1	24.4 ± 0.08	17.6 ± 0.13	17.5 ± 0.2	−0.2	14.1 ± 0.2	0.7
C14- D-leucine C49-D-leucine C66- D-leucine	24.5	35.0 ± 0.2	22.7 ± 0.1	15.7 ± 0.1	19.4 ± 0.3	−0.3	15.8 ± 0.2	0.7

© 2026 The Author(s). Published by the Royal Society of Chemistry

Open Access Article. Published on 10 February 2026. Downloaded on 2/17/2026 2:53:54 PM.
This article is licensed under a Creative Commons Attribution-NonCommercial 3.0 Unported Licence.

Table 3 (*Contd.*)

Carbon nuclei	δ_{iso}(ppm)	δ_{11}(ppm)	δ_{22}(ppm)	δ_{33}(ppm)	Span (ppm)	Skew	Anisotropy ($\Delta\delta$) (ppm)	Asymmetry(η)
C83-D-leucine								
C15, C16-D-leucine (D-leu)	22.5	34.9 ± 0.1	19.5 ± 0.1	13.0 ± 0.1	21.9 ± 0.2	−0.4	18.7 ± 0.2	0.5
C50, C51-D-leucine (D-leu)								
C67, C68-D-leucine (D-leu)								
C84, C85-D-leucine (D-leu)								
C4, C5-L-valine(L-val)	18.5	30.8 ± 0.1	15.9 ± 0.08	8.7 ± 0.1	22.1 ± 0.2	−0.3	18.5 ± 0.2	0.6
C10-D-glycine (D-gly)								
C19-L-alanine (L-ala)								
C23, C24-D-valine (D-val)								
C28, C29-L-valine (L-val)								
C33, C34-D-valine (D-val)								

[a] {Note: The information regarding the anisotropy and the asymmetry of the shielding tensor includes $\{\Delta\delta = \delta_{33} - 1/2(\delta_{11} + \delta_{22})\}$and $\{\eta=(\delta_{22} - \delta_{11})/(\delta_{33} - \delta_{iso})\}$ respectively. The magnitude of the anisotropy defines the distance of the largest separation of the spinning CSA sideband pattern from the position of the center of gravity$\{\delta_{iso} = (\delta_{11} + \delta_{22} + \delta_{33})/3\}$ of the sideband pattern, and the sign of the anisotropy represents on which side of the center of gravity the distance of separation is maximum. The 'asymmetry' parameter indicates the deviation of the spinning CSA sideband pattern from its axially symmetric shape. The 'span' ($\Omega = \delta_{33} - \delta_{11}$) monitors the breadth of the spinning CSA sideband pattern, and 'skew'($k = (\delta_{iso} - \delta_{22})/(\delta_{33} - \delta_{11})$) measures the degree of orientation of the asymmetry pattern. When $k = \pm 1$, the spinning CSA pattern is axially symmetric, and the CS tensor is non-axial when $k = +0.3$.}

and suppress undesired interactions, Phase Modulated Lee-Goldburg (PMLG) decoupling was employed, with systematic optimization of power levels and frequency offsets using the established PMLG sequence.[52,53] By employing a contact time of 0.2 ms, the resulting cross-peaks in the HETCOR spectra predominantly represent through-bond ^{1}H–^{13}C correlations. Notably, stronger ^{1}H–^{13}C dipolar interactions are indicative of reduced molecular mobility or slower dynamic processes.

Fig. 10 represents the heteronuclear correlation spectrum between ^{1}H and ^{13}C, and Table 4 presents the spatial proximity between different carbon and proton nuclei within the 15 amino acid residues of gramicidin A. Gramicidin A is a lipophilic peptide that adopts a left-handed helical structure, where the carbonyl (C═O) groups alternate in orientation—some point toward the amino end, and others toward the carboxyl end of the helix. The C═O groups facing the carboxyl end participate in forming 16-membered hydrogen-bonded rings, while those facing the amino end form 14-membered hydrogen-bonded rings. Two such helices join together to create an ion channel. The alternating orientation of the carbonyl groups allows the helices to pair through hydrogen bonds in both head-to-head and tail-to-tail configurations, enabling stable dimer formation.[19] Notably, the carbonyl group carbons of five different amino acids, valine, glycine, alanine, leucine and tryptophan, exhibit spatial proximity to the proton attached to the nitrogen atom of the pyrrole ring of the indole group of L-tryptophan (1), L-tryptophan (2), L-tryptophan (3), and L-tryptophan (4), and also to the proton connected to the carbon atom residing on the benzene ring of the indole group of L-tryptophan (1), L-tryptophan (2), L-tryptophan (3), and L-tryptophan (4).

The ^{13}C nuclei located on the benzene ring of the indole moiety of L-tryptophan were found to be in close spatial proximity to the proton nuclei attached to the nitrogen atoms of valine, glycine, leucine, and tryptophan residues. This spatial arrangement was further corroborated by NOESY spectra, which revealed distinct inter-residue cross-peaks indicating short through-space distances (as presented in Table 2) between the indole ring of tryptophan and neighboring amino acids. Such proximity underscores the structural importance of tryptophan within the peptide framework. As previously established, tryptophan residues play a crucial role in modulating the hydrophobicity and biological activity of gramicidin A.[54] Thus, the combined insights from NOESY and HETCOR experiments provide compelling microscopic evidence that tryptophan contributes significantly to the stabilization of the polypeptide network. These interactions help define the conformational landscape of the peptide and support its functional properties.

3.5 Determination of spin lattice relaxation time

The quantity $1/T_1$, representing the nuclear spin-lattice relaxation rate, serves as a key probe for electron systems in solids. This parameter reflects the rate at which nuclear spin precession is damped due to interactions with surrounding electron spins. Experimentally, T_1 is determined by monitoring the recovery of the Boltzmann equilibrium magnetization following the application of radiofrequency pulses. The spin-lattice relaxation

Open Access Article. Published on 10 February 2026. Downloaded on 2/17/2026 2:53:54 PM.
This article is licensed under a Creative Commons Attribution-NonCommercial 3.0 Unported Licence.

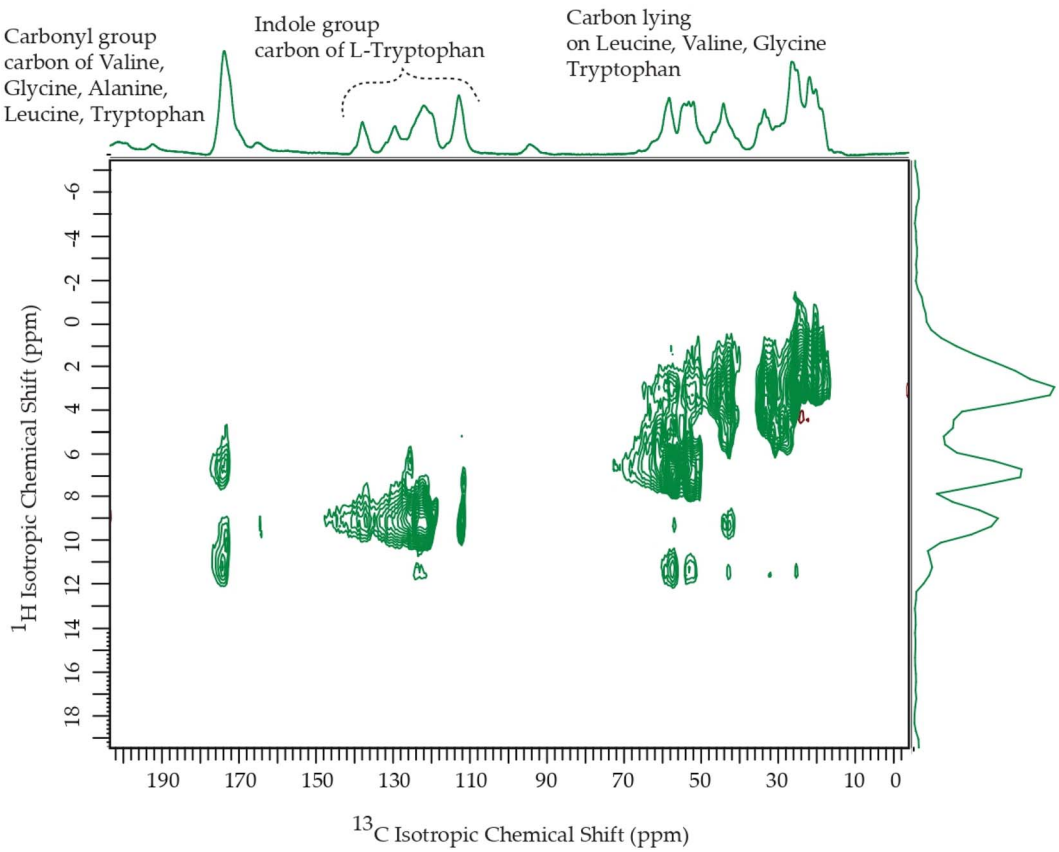

Fig. 10 $^{1}H-^{13}C$ heteronuclear correlation spectrum of gramicidin A.

process is influenced by several mechanisms, including dipole–dipole interactions, quadrupolar coupling, chemical shift anisotropy (CSA), spin-lattice interactions, and spin-diffusion pathways. Each of these contributes to the overall relaxation behavior, offering valuable insight into the local electronic environment and molecular dynamics within the solid. Gramicidin A has a large, hydrophobic, and charge-neutral structure, resulting from its aliphatic/aromatic amino acids and end-capped termini, which enhances its membrane compatibility. Its alternating L- and D-amino acid sequences confer resistance to proteolytic degradation, offering a key advantage over conventional peptides. This stereochemistry also aligns all hydrophobic side chains on one face, facilitating insertion into the hydrophobic core of the lipid bilayer. The dynamic nature of these AMPs was probed by measuring site-specific spin-lattice relaxation time by employing the method devised by Torchia.[27]

The spin-lattice relaxation times for all carbon-13 nuclei in gramicidin A vary from 38 s to 2.5 s, indicating a remarkably high degree of freedom within this linear polypeptide. Such dynamic flexibility plays a crucial role in its biological function, as it enables gramicidin A to efficiently adapt its conformation. This adaptability is particularly important for its ability to integrate into and traverse the lipid bilayer of bacterial membranes. By leveraging its structural flexibility, gramicidin A can effectively penetrate the membrane of target bacteria, ultimately contributing to its antimicrobial activity.

The influence of CSA interaction on the spin-lattice relaxation mechanism is described as follows:[55–58]

$$\frac{1}{T_1^{\mathrm{CSA}}} = \frac{2}{15}\gamma^2 B^2 S^2 \left(\frac{\tau_2}{1+\ \omega^2\tau_2{}^2}\right) \tag{5}$$

where correlation time $\tau_c = 3\ \tau_2$, and B is the applied magnetic field.

$$S^2 = \ (\Delta\delta)^2\left(1+\ \eta^2/3\right) \text{ and } \left[\Delta\delta = \delta_{33} - \ \frac{(\delta_{22}+\delta_{11})}{2}\right],$$

$$\left(\eta = \frac{\delta_{22}-\delta_{11}}{\delta_{33}-\delta_{\mathrm{iso}}}\right)$$

The influence of heteronuclear dipole–dipole coupling on the spin-lattice relaxation mechanism is described by the following:[56]

$$\frac{1}{T_1^{\mathrm{DD}}} = \ \frac{1}{10}\left(\frac{\gamma_{\mathrm{C}}\gamma_{\mathrm{X}}\hbar}{r_{\mathrm{CX}}{}^3}\right)^2 \tau_2 \left[\frac{3}{1+\ \omega_{\mathrm{C}}{}^2\tau_2{}^2} + \frac{1}{1+\ (\omega_{\mathrm{X}}-\omega_{\mathrm{C}})^2\tau_2{}^2} + \frac{6}{1+\ (\omega_{\mathrm{X}}-\omega_{\mathrm{C}})^2\tau_2{}^2}\right] \tag{6}$$

By keeping the first term only,

$$\frac{1}{T_1^{\mathrm{DD}}} = \frac{1}{10}\left(\frac{\gamma_{\mathrm{C}}\gamma_{\mathrm{X}}\hbar}{r_{\mathrm{CX}}{}^3}\right)^2 \tau_2 \left[\frac{3}{1+\ \omega_{\mathrm{C}}{}^2\tau_2{}^2}\right] \tag{7}$$

 © 2026 The Author(s). Published by the Royal Society of Chemistry

Open Access Article. Published on 10 February 2026. Downloaded on 2/17/2026 2:53:54 PM.
This article is licensed under a Creative Commons Attribution-NonCommercial 3.0 Unported Licence.

Table 4 Spatial proximity between the ^{13}C and ^{1}H nuclei of the linear polypeptide gramicidin A, determined by the ^{1}H–^{13}C HETCOR experiment

^{13}C nuclei	^{1}H nuclei
C6-carbonyl group carbon of L-valine (1)	$H10_N$-proton connected to the nitrogen atom of the pyrrole ring of the indole group of L tryptophan (1)
C8-carbonyl group carbon of D-glycine	H43-proton connected to the carbon atom residing on the benzene ring of the indole group of L tryptophan (1)
C11-carbonyl group carbon of L-alanine (1)	$H13_N$-proton connected to the nitrogen atom of the pyrrole ring of the indole group of L tryptophan (2)
C17-carbonyl group carbon of D-leucine (1)	H60-proton connected to the carbon atom residing on the benzene ring of the indole group of L tryptophan (2)
C20-carbonyl group carbon of L-alanine (2)	$H16_N$-proton connected to the nitrogen atom of the pyrrole ring of the indole group of L tryptophan (3)
C25-carbonyl group carbon of D-valine (2)	H77-proton connected to the carbon atom residing on the benzene ring of the indole group of L tryptophan (3)
C30-carbonyl group carbon of L-valine (3)	$H19_N$-proton connected to the nitrogen atom of the pyrrole ring of the indole group of L tryptophan (4)
C35-carbonyl group carbon of D-valine (4)	H94-proton connected to the carbon atom residing on the benzene ring of the indole group of L tryptophan (4)
C46-carbonyl group carbon of L-tryptophan (1)	
C52-carbonyl group carbon of D-leucine (2)	
C63-carbonyl group carbon of L-tryptophan (2)	
C69-carbonyl group carbon of D-leucine (3)	
C80-carbonyl group carbon of L-tryptophan (3)	
C86-carbonyl group carbon of D-leucine (4)	
C97-carbonyl group carbon of L-tryptophan (4)	
C40-carbon nuclei residing on the benzene ring of the indole group of L-tryptophan (1)	$H1_N$-proton bonded to nitrogen atom N1 of L-valine (1)
C57-carbon nuclei residing on the benzene ring of the indole group of L-tryptophan (2)	$H2_N$-proton bonded to nitrogen atom N2 of D-glycine
C74-carbon nuclei residing on the benzene ring of the indole group of L-tryptophan (3)	$H4_N$-proton bonded to nitrogen atom N4 of D-leucine (1)
C91-carbon nuclei residing on the benzene ring of the indole group of L-tryptophan (4)	$H6_N$-proton bonded to nitrogen atom N6 of D-valine (2)
C45-carbon nuclei residing on the benzene ring of the indole group of L-tryptophan (1)	$H7_N$-proton bonded to nitrogen atom N7 of L-valine (3)
C79-carbon nuclei residing on the benzene ring of the indole group of L-tryptophan (3)	$H8_N$-proton bonded to nitrogen atom N8 of D-valine (4)
C96-carbon nuclei residing on the benzene ring of the indole group of L-tryptophan (4)	$H9_N$-proton bonded to nitrogen atom N9 of L-tryptophan (1)
C39-carbon nuclei residing on the pyrrole ring of the indole group of L-tryptophan (1)	$H11_N$-proton bonded to nitrogen atom N11 of D-leucine (2)
C56-carbon nuclei residing on the pyrrole ring of the indole group of L-tryptophan (2)	$H12_N$-proton bonded to nitrogen atom N12 of L-tryptophan (2)
C73-carbon nuclei residing on the pyrrole ring of the indole group of L-tryptophan (3)	$H14_N$-proton bonded to nitrogen atom N14 of D-leucine (3)
C90-carbon nuclei residing on the pyrrole ring of the indole group of L-tryptophan (4)	$H15_N$-proton bonded to nitrogen atom N15 of L-tryptophan (3)

Open Access Article. Published on 10 February 2026. Downloaded on 2/17/2026 2:53:54 PM.
This article is licensed under a Creative Commons Attribution-NonCommercial 3.0 Unported Licence.

Table 4 (*Contd.*)

^{13}C nuclei	^{1}H nuclei
C62-carbon nuclei residing on the benzene ring of the indole group of L-tryptophan (2)	$H17_N$-proton bonded to nitrogen atom N17 of D-leucine (4)
C96-carbon nuclei residing on the benzene ring of the indole group of L-tryptophan (4)	$H18_N$-proton bonded to nitrogen atom N18 of L-tryptophan (4)
C42, C43, C44-carbon nuclei residing on the benzene ring of the indole group of L-tryptophan (1)	$H9_N$-proton bonded to nitrogen atom N9 of L-tryptophan (1) H43-proton connected to the carbon atom residing on the benzene ring of the indole group of L-tryptophan (1)
C59, C60, C61-carbon nuclei residing on the benzene ring of the indole group of L-tryptophan (2)	$H12_N$-proton bonded to the nitrogen atom N12 of L-tryptophan (2) H60-proton connected to the carbon atom residing on the benzene ring of the indole group of L-tryptophan (2)
C76, C77, C78-carbon nuclei residing on the benzene ring of the indole group of L-tryptophan (3)	$H15_N$-proton bonded to the nitrogen atom N15 of L-tryptophan (3) H77-proton connected to the carbon atom residing on the benzene ring of the indole group of L-tryptophan (3)
C93, C94, C95-carbon nuclei residing on the benzene ring of the indole group of L-tryptophan (4)	$H18_N$-proton bonded with nitrogen atom N18 of L-tryptophan (4) H94-proton connected to the carbon atom residing on the benzene ring of the indole group of L-tryptophan (4)
C38, C41-carbon nuclei residing on the indole group of L-tryptophan (1)	$H9_N$-proton bonded to the nitrogen atom N9 of L-tryptophan (1) H43-proton connected to the carbon atom residing on the benzene ring of the indole group of L-tryptophan (1)
C55, C58-carbon nuclei residing on the indole group of L-tryptophan (2)	$H12_N$-proton bonded to the nitrogen atom N12 of L-tryptophan (2) H60-proton connected to the carbon atom residing on the benzene ring of the indole group of L-tryptophan (2)
C72, C75-carbon nuclei residing on the indole group of L-tryptophan (3)	$H15_N$-proton bonded to nitrogen atom N15 of L-tryptophan (3) H77-proton connected to the carbon atom residing on the benzene ring of the indole group of L-tryptophan (3)
C89, C92-carbon nuclei residing on the indole group of L-tryptophan (4)	$H18_N$-proton bonded to nitrogen atom N18 of L-tryptophan (4) H94-proton connected to the carbon atom residing on the benzene ring of the indole group of L-tryptophan (4)
C2-carbon nuclei residing on the amino acid L-valine (1) bonded to nitrogen N1	H39-proton bonded to the pyrrole ring of L-tryptophan (1)
C12-carbon nuclei residing on the amino acid D-leucine(1) bonded to nitrogen N4	H42-proton bonded to the benzene ring of L-tryptophan (1)
C21-carbon nuclei residing on the amino acid D-valine (2) bonded to N6	H43-proton bonded to the benzene ring of L-tryptophan (1)
C26-carbon nuclei residing on the amino acid L-valine (3) bonded to N7	
C31-carbon nuclei residing on the amino acid D-valine (4) bonded to N8	
C36-carbon nuclei residing on the amino acid L-tryptophan (1) bonded to N9	
C47-carbon nuclei residing on the amino acid D-leucine(2) bonded to N11	
C53-carbon nuclei residing on the amino acid L-tryptophan (2) bonded to N12	H56-proton bonded to the pyrrole ring of L-tryptophan (2)
C64-carbon nuclei residing on the amino acid D-leucine (3) bonded to N14	H59-proton bonded to the benzene ring of L-tryptophan (2) H60-proton bonded to the benzene ring of L-tryptophan (2)
C70-carbon nuclei residing on the amino acid L-tryptophan (3) bonded to N15	H73-proton bonded to the pyrrole ring of L-tryptophan (3) H76-proton bonded to the benzene ring of L-tryptophan (3) H77-proton bonded to the benzene ring of L-tryptophan (3)
C81-carbon nuclei residing on the amino acid D-leucine (4) bonded to N17	H90-proton bonded to the pyrrole ring of L-tryptophan (4)
C87-carbon nuclei residing on the amino acid L-tryptophan (4) bonded to N18	H93-proton bonded to the benzene ring of L-tryptophan (4)
C99-carbon nuclei residing on the molecular moiety ethanolamine ($NHCH_2CH_2OH$) bonded to N20	H94-proton bonded to the benzene ring of L-tryptophan (4)

© 2026 The Author(s). Published by the Royal Society of Chemistry

Open Access Article. Published on 10 February 2026. Downloaded on 2/17/2026 2:53:54 PM.
This article is licensed under a Creative Commons Attribution-NonCommercial 3.0 Unported Licence.

Table 4 (*Contd.*)

^{13}C nuclei	^{1}H nuclei
C9-carbon nuclei residing on the amino acid L-alanine (1)	H90-proton bonded to the pyrrole ring of L-tryptophan (4)
	H93-proton bonded to the benzene ring of L-tryptophan (4)
	H94-proton bonded to the benzene ring of L-tryptophan (4)
C18-carbon nuclei residing on the amino acid L-alanine (2)	H39-proton bonded to the pyrrole ring of L-tryptophan (1)
	H42-proton bonded to the benzene ring of L-tryptophan (1)
	H43-proton bonded to the benzene ring of L-tryptophan (1)
C7-carbon nuclei residing on the amino acid D-glycine	H3-proton attached to C3 of L-valine (1)
C13-carbon nuclei residing on the amino acid D-leucine (1)	H22-proton attached to C22 of D-valine (2)
C48-carbon nuclei residing on the amino acid D-leucine (2)	H54-proton attached to C54 of L-tryptophan (2)
	H37-proton attached to C37 of L-tryptophan (1)
	H32-proton attached to C32 of D-valine (4)
C65-carbon nuclei residing on the amino acid D-leucine (3)	H71-proton attached to C71 of L-tryptophan (3)
C82-carbon nuclei residing on the amino acid D-leucine (4)	H88-proton attached to C88 of L-tryptophan (4)
C98-carbon nuclei residing on the molecular moiety ethanolamine ($NHCH_2CH_2OH$)	H98-proton attached to C98 of ethanolamine
	H88-proton attached to C88 of L-tryptophan (4)
C22-carbon nuclei residing on the amino acid D-valine (2)	H22-proton on D-valine (2)
C27-carbon nuclei residing on the amino acid L-valine (3)	H27-proton on L-valine (3)
C32-carbon nuclei residing on the amino acid D-valine (4)	H32-proton on D-valine (4)
C37-carbon nuclei residing on the amino acid L-tryptophan (1)	H37-proton on L-tryptophan (1)
	H32-proton on D-valine (4)
C54-carbon nuclei residing on the amino acid L-tryptophan (2)	H54-proton residing on L-tryptophan (2)
C88- carbon nuclei residing on the amino acid L-tryptophan (4)	H88-proton residing on L-tryptophan (4)
C71-carbon nuclei residing on the amino acid L-tryptophan (3)	H71-proton residing on L-tryptophan (3)
C14-carbon nuclei residing on the amino acid D-leucine (1)	H13-proton on D-leucine (1)
	H10-proton on L-alanine (1)
C49-carbon nuclei residing on the amino acid D-leucine (2)	H37-proton on L-tryptophan (1)
C66-carbon nuclei residing on the amino acid D-leucine (3)	H71-proton on L-tryptophan (3)
	H54-proton on L-tryptophan (2)
C83-carbon nuclei residing on the amino acid D-leucine (4)	H88-proton on L-tryptophan (4)
C15, C16-methyl group carbon nuclei residing on the amino acid D-leucine (1)	H19-proton on L-alanine (2)
C50, C51-methyl group carbon nuclei residing on the amino acid D-leucine (2)	H54-proton on L-tryptophan (2)
C67, C68-methyl group carbon nuclei residing on the amino acid D-leucine (3)	H71-proton on L-tryptophan (3)
C84, C85-methyl group carbon nuclei residing on the amino acid D-leucine (4)	H88-proton on L-tryptophan (4)
C4, C5-methyl group carbon nuclei residing on the amino acid L-valine(1)	H3-proton on L-valine (1)
C10-methyl group carbon nuclei residing on the amino acid L-alanine (1)	H10-proton on L-alanine (1)
C19-methyl group carbon nuclei residing on the amino acid L-alanine (2)	H19-proton on L-alanine (2)
C23, C24-methyl group carbon nuclei residing on the amino acid D-valine (2)	H22-proton on D-valine (2)
C28, C29-methyl group carbon nuclei residing on the amino acid L-valine (3)	H27-proton on L-valine (3)
C33, C34-methyl group carbon nuclei residing on the amino acid D-valine (4)	H32-proton on D-valine (4)

© 2026 The Author(s). Published by the Royal Society of Chemistry

Open Access Article. Published on 10 February 2026. Downloaded on 2/17/2026 2:53:54 PM.
This article is licensed under a Creative Commons Attribution-NonCommercial 3.0 Unported Licence.

Table 5 Spin-lattice relaxation time and local correlation time at various carbon nuclei sites of gramicidin A

Carbon nuclei	Isotropic chemical shift	Spin-lattice relaxation time (s)	Local correlation time (s)
Carbonyl group carbon of valine, glycine, alanine, leucine, tryptophan (C6, C8, C11, C17, C20, C25, C30, C35, C46, C52, C63, C69, C80, C86, C97)	173.8	38 ± 1	4.8×10^{-5}
Carbon nuclei of the formyl group (C1)	165.0	35 ± 1	4.5×10^{-5}
Carbon nuclei residing on the indole group of L-tryptophan (C40, C57, C74, C91)	137.8	38 ± 1	7.5×10^{-5}
Carbon nuclei residing on the indole group of L-tryptophan (C45, C62, C79, C96)	129.4	18 ± 1	4.1×10^{-5}
Carbon nuclei residing on the indole group of L-tryptophan (C39, C56, C73, C90)	123.0	14 ± 1	3.6×10^{-5}
Carbon nuclei residing on the indole group of L-tryptophan (C42, C43, C44, C59, C60, C61, C76, C77, C78, C93, C94, C95)	121.9	14 ± 1	3.6×10^{-5}
Carbon nuclei residing on the indole group of L-tryptophan (C38, C41, C55, C58, C72, C75, C89, C92)	112.6	20 ± 3	3.1×10^{-5}
C2-L-valine; C12-D-leucine	57.9	25 ± 1	1.9×10^{-6}
C21-D-valine			
C26-L-valine; C31-D-valine			
C36-L-tryptophan; C47-D-leucine			
C53-L-tryptophan; C64-D-leucine			
C70-L-tryptophan; C81-D-leucine			
C8 -L-tryptophan			
C99-carbon nuclei residing on the molecular moiety ethanolamine ($NHCH_2CH_2OH$)			
C9, C18-carbon nuclei residing on the amino acid L-alanine(L-ala)	54.1	20 ± 1	1.8×10^{-6}
C7-D-glycine	43.7	7 ± 1	3.1×10^{-7}
C13-D-leucine			
C48-D-leucine			
C65-D-leucine			
C82-D-leucine			
C98- carbon nuclei residing on the molecular moiety ethanolamine ($NHCH_2CH_2OH$)			
C22-D-valine	33.0	5.5 ± 0.5	1.2×10^{-7}
C27-L-valine			
C32-D-valine			
C37-L-tryptophan	25.7	3.0 ± 0.5	5.5×10^{-8}
C54-L-tryptophan			
C88-L-tryptophan			
C71-L-tryptophan			
C14-D-leucine	24.5	2.5 ± 0.5	5.8×10^{-8}
C49-D-leucine			
C66-D-leucine			
C83-D-leucine			
C15, C16-D-leucine	22.5	2.5 ± 0.5	7.6×10^{-8}
C50, C51-D-leucine			
C67, C68-D-leucine			
C84, C85-D-leucine			
C4, C5-L-valine (L-val)	18.5	2.5 ± 0.5	7.6×10^{-8}
C10- D-glycine (D-gly)			
C19-L-alanine (L-ala)			
C23, C24-D-valine (D-val)			
C28, C29-L-valine (L-val)			
C33, C34-D-valine (D-val)			

© 2026 The Author(s). Published by the Royal Society of Chemistry

Open Access Article. Published on 10 February 2026. Downloaded on 2/17/2026 2:53:54 PM.
This article is licensed under a Creative Commons Attribution-NonCommercial 3.0 Unported Licence.

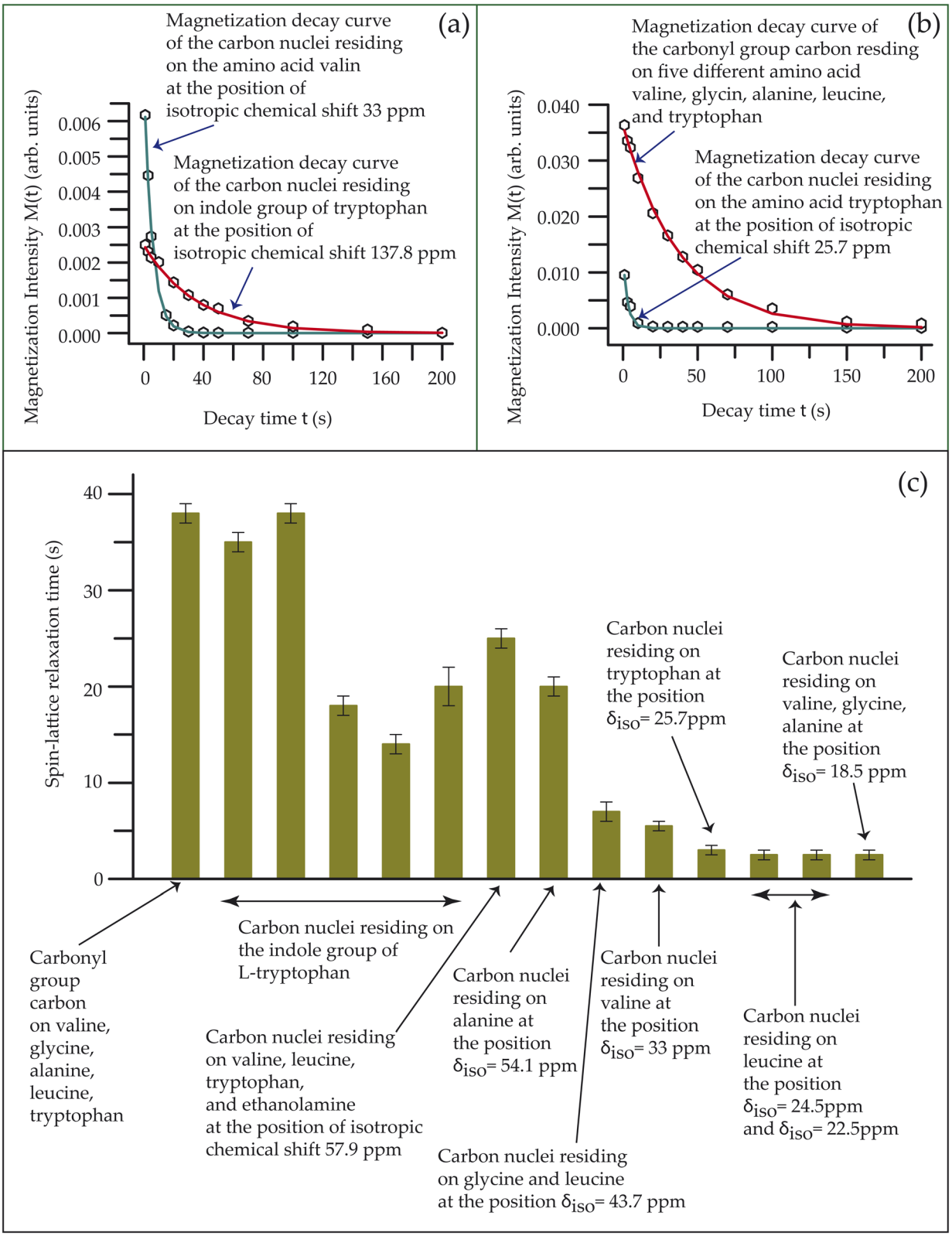

Fig. 11 (a and b) The magnetization decay curves of various carbon nuclei residing on gramicidin A. (c) A bar-diagram of the spin-lattice relaxation times of various carbon nuclei.

Open Access Article. Published on 10 February 2026. Downloaded on 2/17/2026 2:53:54 PM.
This article is licensed under a Creative Commons Attribution-NonCommercial 3.0 Unported Licence.

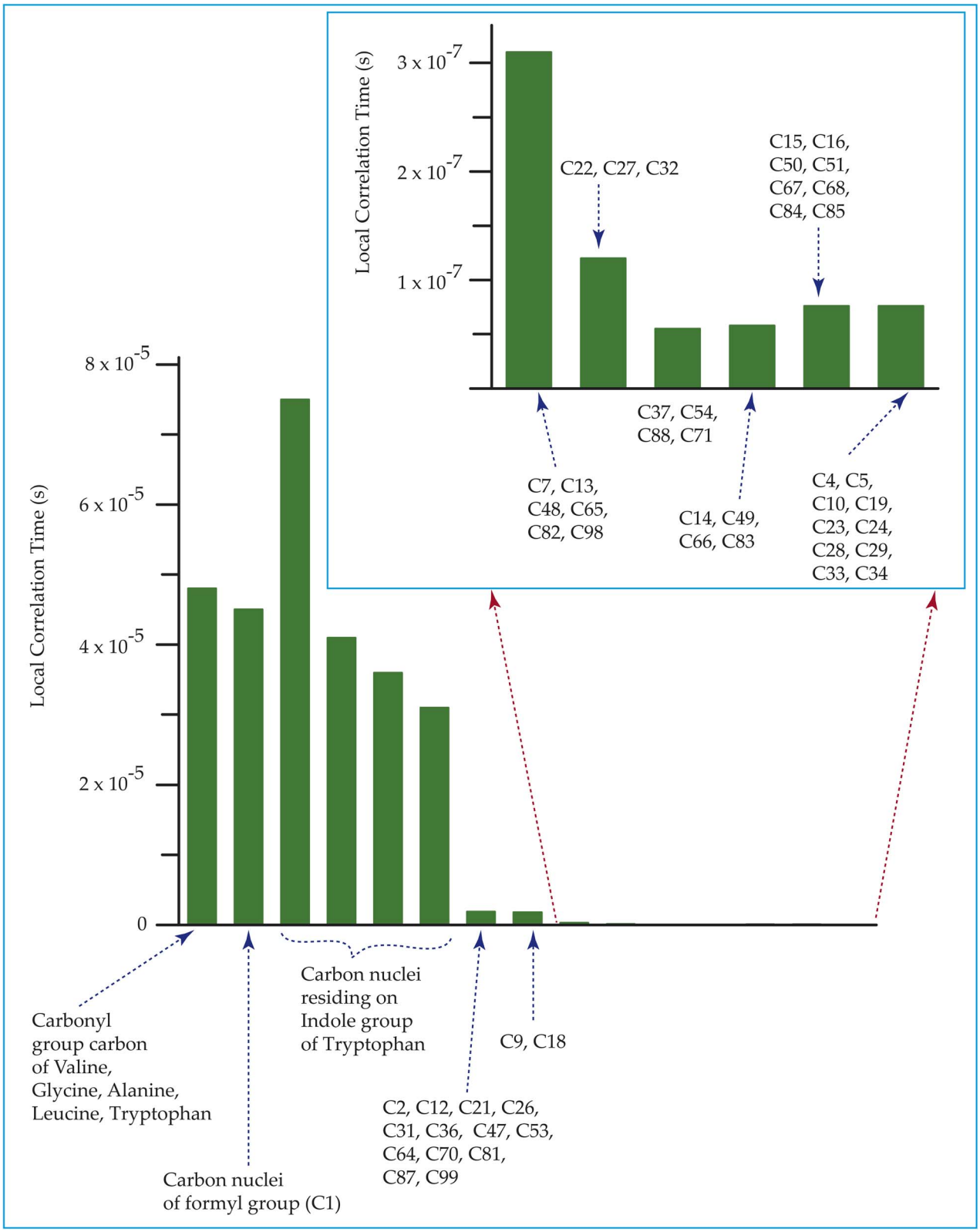

Fig. 12 Bar-diagram of the local rotational correlation times of various carbon nuclei on gramicidin A. It varies from 5.5×10^{-8} s to 7.5×10^{-5} s. The local correlation time of the carbon nuclei residing on the indole group of tryptophan residue is the longest among the amino acid residues.

 © 2026 The Author(s). Published by the Royal Society of Chemistry

Open Access Article. Published on 10 February 2026. Downloaded on 2/17/2026 2:53:54 PM.
This article is licensed under a Creative Commons Attribution-NonCommercial 3.0 Unported Licence.

X refers to hydrogen, oxygen, or nitrogen, and r_{CX} signifies the separation between the carbon atom and its neighboring hydrogen, oxygen, or nitrogen atoms. The Larmor precession frequency

$$\omega = 2\pi f = 2 \times 3.14 \times 125.758 \text{ MHz} = 789.76024 \text{ MHz};$$
$$B = 11.74\ T$$

$$\gamma_C = 10.7084 \text{ MHz } T^{-1},\ \gamma_H = 42.577 \text{ MHz } T^{-1},$$
$$\hbar = 1.054 \times 10^{-34}\ Js$$

The spin-lattice relaxation rate for ^{13}C can be written as follows:

$$\frac{1}{T_1} = \frac{1}{T_1^{CSA}} + \frac{1}{T_1^{DD}} = \frac{2}{15}\gamma^2 B^2 S^2 \left(\frac{\tau_2}{1+\omega^2\tau_2{}^2}\right) + \frac{1}{10}\left(\frac{\gamma_C\gamma_X\hbar}{r_{CX}{}^3}\right)^2 \tau_2 \left[\frac{3}{1+\omega_C{}^2\tau_2{}^2}\right] \quad (8)$$

The rotational correlation times at different carbon nuclei locations in gramicidin A can be evaluated through this expression.

A significant difference in nuclear spin dynamics was observed among various carbon nuclei, as shown in Table 5, Fig. 11 and 12. The local correlation times of aliphatic ^{13}C nuclei belonging to residues such as leucine, valine, glycine, and alanine fall within the range of 10^{-6} s to 10^{-8} s, indicative of their relatively rapid motional dynamics. In contrast, the ^{13}C nuclei located on the indole ring of L-tryptophan, as well as those of carbonyl groups, exhibit substantially longer correlation times of the order of 10^{-5} s, reflecting their more restricted molecular motion. This reduced mobility is consistent with the structural and functional role of tryptophan in the polypeptide antibiotic gramicidin A. Tryptophan is unique among the proteinogenic amino acids, possessing a bi-cyclic aromatic indole system composed of a benzene ring fused to a pyrrole ring. The indole moiety participates in a variety of noncovalent interactions: π–π stacking with other aromatic residues, hydrogen bonding *via* the NH group of the pyrrole ring, and hydrophobic, as well as cation-π, interactions involving the benzene ring. Collectively, these interactions are crucial in shaping the three-dimensional architecture, functional properties, and biological activity of tryptophan-containing peptides.

The pronounced difference in correlation times arises from the distinct molecular environments and degrees of motional freedom associated with these carbon sites. Aliphatic methyl carbons experience relatively unrestricted rotation and minimal steric hindrance, leading to their faster dynamics. In contrast, carbonyl carbons are conformationally constrained due to their involvement in intra- and intermolecular hydrogen bonding. The carbonyl oxygen of one residue typically forms a hydrogen bond with the amide hydrogen of another, contributing to the stabilization of secondary structural motifs such as helices and β-turns. This hydrogen-bonding network imparts rigidity to the peptide backbone, thereby suppressing the motion of carbonyl groups. The resulting restricted mobility manifests in slower nuclear spin dynamics of the carbonyl ^{13}C nuclei, as observed in the solid-state NMR measurements.

Another reason for this variation of nuclear spin-dynamics arises due to the variation of the principal components of the CSA parameters. As discussed in the previous section, the principal components of the chemical shift anisotropy (CSA) tensor are substantially higher for carbonyl carbons and aromatic carbons belonging to the L-tryptophan residue than other aliphatic carbons of the polypeptide. This increase is attributed to the presence of hydrogen bonds, which influence the electronic environment and chemical shift anisotropy parameters. The spin-lattice relaxation time of ^{13}C nuclei is largely governed by two primary relaxation mechanisms: heteronuclear dipole–dipole interactions (primarily with nearby protons) and CSA interactions. In the case of non-protonated carbons, such as those in carbonyl groups, the relaxation is predominantly driven by CSA interactions, particularly at high magnetic fields. Therefore, for both carbonyl carbons and the aromatic carbon nuclei within the indole ring of L-tryptophan, substantially higher values of the CSA parameters are directly associated with slower motional dynamics. This underscores a clear relationship between the electronic environment, molecular motion, and nuclear spin relaxation behaviour in peptides. Such systematic approaches, which leverage high-resolution NMR measurements to obtain detailed structural and dynamical information at the atomic scale, will substantially advance the emerging field of NMR crystallography. Moreover, these methodologies will provide a rational framework for molecular editing strategies aimed at optimizing the physicochemical and biological properties of tryptophan-containing peptide antibiotics.

4. Conclusion

The resonance lines in the ^1H and ^{13}C liquid-state NMR spectra of the linear peptide antibiotic gramicidin A were assigned using a series of two-dimensional (2D) NMR techniques, including ^1H–^{13}C HSQC, ^1H–^{13}C HMBC, ^1H–^1H COSY, and ^1H–^1H TOCSY experiments, and compared with those of the previously reported article published by G. E. Hawkes and coworkers.[35] Spatial proximity and internuclear distances between protons associated with various amino acids were extracted by using 2D ^1H–^1H NOESY NMR. To explore the detailed structural and nuclear spin dynamics of gramicidin A, the principal components of the chemical shift anisotropy (CSA) parameters, spin-lattice relaxation times, and local correlation times at various ^{13}C sites were extracted by deploying solid-state NMR measurements. CSA values were determined through ^{13}C 2D PASS CP-MAS solid-state NMR experiments, while site-specific spin-lattice relaxation times were measured using the method developed by Torchia.[27] Relaxation time measurements revealed a high degree of internal motion in this linear polypeptide, indicating considerable molecular flexibility. This dynamic nature allows gramicidin A to adapt its conformation and efficiently insert into and traverse the lipid bilayer of bacterial membranes—a key feature underpinning its antimicrobial activity.

Open Access Article. Published on 10 February 2026. Downloaded on 2/17/2026 2:53:54 PM.
This article is licensed under a Creative Commons Attribution-NonCommercial 3.0 Unported Licence.

Tryptophan, owing to its amphipathic nature and aromatic indole ring, exhibits strong interactions with bacterial membranes. These interactions promote membrane destabilization and facilitate the anchoring and penetration mechanisms characteristic of antimicrobial peptides (AMPs). Consequently, tryptophan residues play a pivotal role in governing the membrane-disrupting capability and overall antimicrobial efficacy of AMPs. Our solid-state NMR measurements reveal that the chemical shift anisotropy (CSA) parameters are markedly elevated for the ^{13}C nuclei located within the indole ring of L-tryptophan. This enhancement arises from pronounced magnetic shielding and deshielding effects intrinsic to the aromatic microenvironment. Additionally, the carbon nuclei on the indole side chain exhibit relatively long local correlation times—of the order of 10^{-5} s —indicating restricted motional dynamics.

Thus, while functional activity is not directly assessed, the combined solution and solid-state NMR data provide site-specific structure and local nuclear spin-dynamics at each carbon nucleus site of the linear polypeptide antibiotic, which are closely linked to the functional state of gramicidin A, thereby contributing to an improved understanding of its membrane-associated behaviour within the framework of NMR crystallography.

Conflicts of interest

There are no conflicts to declare.

Data availability

All data obtained from both liquid- and solid-state NMR experiments are presented in this manuscript. Additional information can be provided upon request.

Supplementary information (SI): (i) detailed description of the solid and liquid NMR experiment; (ii) comparison of the assignment of ^{1}H and ^{13}C liquid NMR spectra of the current work with that of the previously published article by Howkes *et al.* {Hawkes, G. H.; Lian, L. Y.; Randall, E. W.; Sales, K. D.; Curzon, E. H. The conformation of gramicidin A in dimethylsulphoxide solution: A full analysis of the one-and two-dimensional ^{1}H, ^{13}C, and ^{15}N nuclear-magnetic-resonance spectra. *Eur. J. Biochem.*, 1987, 166(2), 437–445} in both tabulated form and linear fitting; (iii) 1H–1H NOESY spectra at mixing times of 0.1, 0.2, 0.5 and 0.6 s; (iv) assignment of ^{1}H and ^{13}C liquid NMR spectra in a tabulated form; (v) 2D ^{1}H–^{13}C HSQC spectrum of gramicidin A, and the corresponding assignment of cross peak in a tabulated form; (vi) 2D ^{1}H–^{13}C HMBC NMR spectrum of gramicidin A, and the corresponding assignment of cross peak in tabulated form; (vii) 2D ^{1}H–^{1}H COSY spectrum of gramicidin A, and the corresponding assignment of cross peak in tabulated form; (viii) 2D ^{1}H–^{1}H TOCSY NMR spectrum of gramicidin A, and the corresponding assignment of cross peak in tabulated form; (ix) variation of NOE intensity and internuclear distance between two spatially close protons with different mixing time; and (x) assignment of ^{13}C CP-MAS SSNMR spectrum of gramicidin A. See DOI: https://doi.org/10.1039/d5ra09180b.

Acknowledgements

The author Manasi Ghosh is grateful to the Science and Engineering Research Board (SERB)-POWER research grant (file no. SPG/2021/000303), Department of Science and Technology (DST), Government of India, and the IoE-BHU Seed Grant-II (Dev. Scheme No. 6031(B) for financial support. The authors are thankful to Dr. Harisingh Gour University for providing the 500 MHz solid-state NMR facility and Banaras Hindu University for providing the 600 MHz liquid NMR facility.

References

1 C. O. Gualerzi, L. Brandi, A. Fabbretti and C. L. Pon, *Antibiotics: Targets, Mechanisms and Resistance*, Wiley-VCH, 2013.
2 J. Poehlsgaard and S. Douthwaite, The bacterial ribosome as a target for antibiotics, *Nat. Rev. Microbiol.*, 2005, **3**, 870–881.
3 M. N. Alekshun and S. B. Levy, Molecular mechanisms of antibacterial multidrug resistance, *Cell*, 2007, **128**, 1037–1050.
4 J. M. Munita and C. A. Arias, Mechanisms of Antibiotic Resistance, *Microbiol. Spectr.*, 2016, **4**, 1–24.
5 M. Masi, M. Refregiers, K. M. Pos and J. M. Pages, Mechanisms of envelope permeabilityand antibiotic influx and efflux in Gram-negative bacteria, *Nat. Microbiol.*, 2017, **2**, 17001.
6 M. Zasloff, Antimicrobial peptides of multicellular organisms: my perspective, *Adv. Exp. Med. Biol.*, 2019, **1117**, 3–6.
7 M. Zasloff, Antimicrobial peptides of multicellular organisms, *Nature*, 2002, **415**, 389–395.
8 A. Peschel, How do bacteria resist human antimicrobial peptides?, *Trends Microbiol.*, 2002, **10**, 179–186.
9 Z. Wang and G. Wang, APD: the antimicrobial peptide database, *Nucleic Acids Res.*, 2004, **32**, D590–D592.
10 R. J. Dubos, Studies on a bactericidal agent extracted from a soil Bacillus, *J. Exp. Med.*, 1939, **70**, 1–10.
11 R. D. Hotchkiss and R. J. Dubos, Fractionation of the bactericidal agent fromcultures of a soil Bacillus, *J. Biol. Chem.*, 1940, **132**, 791–792.
12 W. E. Herrell and D. Heilman, Experimental and clinical studies on gramicidin, *J. Clin. Invest.*, 1941, **20**, 583–591.
13 H. J. Robinson and H. Molitor, Some toxicological and pharmacological properties of gramicidin, tyrocidine and tyrothricin, *J. Pharmacol. Exp. Ther.*, 1942, **74**, 75–82.
14 B. L. Zerfas, Y. Joo and Y. J. Gao, Gramicidin A mutants with antibiotic activity against both Gram-positive and Gram-negative bacteria, *ChemMedChem*, 2016, **11**, 629–636.
15 A. Knopik-Skrocka and J. Bielawski, The mechanism of the hemolytic activity of polyene antibiotics, *Cell. Mol. Biol. Lett.*, 2002, **7**, 31–48.
16 J. M. David, T. A. Owens, S. P. Barwe and A. K. Rajasekaran, Gramicidin A induces metabolic dysfunction and energy depletion leading to cell death in renal cell carcinoma cells, *Mol. Cancer Ther.*, 2013, **12**, 2296–2307.
17 W. D. Stein and T. Litman, Channels, Carriers, and Pumps, *An Introduction to Membrane Transport, Chapter 3- Ion Channels across Cell Membranes*, 2nd edn, 2015, pp. 81–130.

 © 2026 The Author(s). Published by the Royal Society of Chemistry

Open Access Article. Published on 10 February 2026. Downloaded on 2/17/2026 2:53:54 PM.
This article is licensed under a Creative Commons Attribution-NonCommercial 3.0 Unported Licence.

18 D. W. Urry, M. C. Goodall, J. D. Glickson and D. F. Mayers, The Gramicidin A Transmembrane Channel: Characteristics of Head-to-Head Dimerized π(LD) Helices, *Proc. Natl. Acad. Sci. USA*, 1971, **68**, 1907–1911.
19 D. W. Urry, The Gramicidin A Transmembrane Channel: A Proposed π(LD) Helix, *Proc. Natl. Acad. Sci. USA*, 1971, **68**, 672–676.
20 E. T. Fossel, W. R. Veatch, Y. A. Ovchinnikov and E. R. Blout, A 13C Nuclear Magnetic Resonance Study of Gramicidin A in monomer and dimer forms, *Biochemistry*, 1974, **13**, 5264–5275.
21 P. O. Quist, 13C solid-state NMR of gramicidin A in a lipid membrane, *Biophys. J.*, 1998, **75**, 2478–2488.
22 R. R. Ketchem, K. C. Lee, S. Huo and T. A. Cross, Macromolecular structural elucidation with solid-state NMR-derived orientational constraints, *J. Biomol. NMR*, 1996, **8**, 1–14.
23 W. Zhang, T. Sato and S. O. Smith, NMR spectroscopy of basic/aromatic amino acid clusters in membrane proteins, *Prog. Nucl. Magn. Reson. Spectrosc.*, 2006, **48**, 183–199.
24 D. A. Kelkar and A. Chattopadhyay, A gramicidin ion channel: a model membrane protein, *Biochim. Biophys. Acta*, 2007, **1768**, 2011–2025.
25 T. W. Allen, O. S. Andersen and B. Roux, structure of gramicidin A in a lipid bilayer environment determined using molecular dynamics simulations and solid-state NMR data, *J. Am. Chem. Soc.*, 2003, **125**, 9868–9877.
26 R. E. Koeppe, H. Sun, P. C. A. van der Wel, M. Erin, E. M. Scherer, P. Pulay and D. V. Greathouse, Combined Experimental/Theoretical Refinement of Indole Ring Geometry Using Deuterium Magnetic Resonance and ab Initio Calculations, *J. Am. Chem. Soc.*, 2003, **125**, 12268–12276.
27 D. A. Torchia, The measurement of proton-enhanced carbon-13 T1 values by method which suppresses artifacts, *J. Magn. Reson.*, 1978, **30**, 613–616.
28 L. Lodhi, J. P. Yadav, T. Yamazaki, N. T. Duong, S. L. Poojary, K. K. Dey, Y. Nishiyama and M. Ghosh, NMR Crystallographic Approach to Study the Variation of the Dynamics of Quinine and its Quasienantimer Quinidine, *J. Phys. Chem. C*, 2022, **126**, 17291–17305.
29 J. P. Yadav, L. Lodhi, T. Fatma, K. K. Dey and M. Ghosh, Investigation of the Influence of Various Functional Groups on the Dynamics of Glucocorticoids, *ACS Omega*, 2022, **7**, 43190–43209.
30 K. K. Dey, M. M. Deshmukh and M. Ghosh, A Description of the Local Structure and Dynamics of Ketoconazole Molecule by Solid-State NMR Measurements and DFT Calculations: Proposition for NMR Crystallography, *ChemistrySelect*, 2021, **6**, 10208–10220.
31 K. K. Dey, L. Lodhi and M. Ghosh, Study of the Variation of the Electronic Distribution and Motional Dynamics of Two Independent Molecules of an Asymmetric Unit of Atorvastatin Calcium by Solid-State NMR Measurements, *ACS Omega*, 2021, **6**, 22752–22764.
32 K. K. Dey and M. Ghosh, Understanding the Effect of an Anionic Side-Chain on the Nuclear Spin Dynamics of a Polysaccharide, *Cellulose*, 2022, **29**, 1381–1392.
33 W. T. Dixon, Spinning-sideband-free and spinning-sideband only NMR spectra in spinning samples, *J. Chem. Phys.*, 1982, **77**, 1800–1809.
34 O. N. Antzutkin, S. C. Shekar and M. H. Levitt, Two-dimensional sideband separation in magic angle spinning NMR, *J. Magn. Reson., Ser. A*, 1995, **115**, 7–19.
35 G. H. Hawkes, L. Y. Lian, E. W. Randall, K. D. Sales and E. H. Curzon, The conformation of gramicidin A in dimethylsulphoxide solution: A full analysis of the one-and two-dimensional ^{1}H, ^{13}C, and ^{15}N nuclear-magnetic-resonance spectra, *Eur. J. Biochem.*, 1987, **166**(2), 437–445.
36 S. S. Golotvin, E. Vodopianov, R. Pol, B. A. Lefebvre, A. J. Williams, R. D. Rutkowske and T. D. Spitzer, Automated structure verification based on a combination of 1D 1H NMR and 2D 1H-13C HSQC spectra, *Magn. Reson. Chem.*, 2007, **45**(10), 803–813.
37 M. Pérez-Trujillo, P. Nolis and T. Parella, CN-HMBC: A powerful NMR technique for the simultaneous detection of long-range 1H, 13C and 1H, 15N connectivities, *Org. Lett.*, 2007, **9**(1), 29–32.
38 D. Marion and K. Wüthrich, Application of phase sensitive two-dimensional correlated spectroscopy (COSY) for measurements of 1H-1H spin-spin coupling constants in proteins, *Biochem. Biophys. Res. Commun.*, 1983, **113**(3), 967–974.
39 K. Bingol, L. Bruschweiler-Li, D. W. Li and R. Bruschweiler, Customized metabolomics database for the analysis of NMR 1H–1H TOCSY and 13C–1H HSQC-TOCSY spectra of complex mixtures, *Anal. Chem.*, 2014, **86**(11), 5494–5501.
40 A. B. Sebag, R. N. Hanson, D. A. Forsyth and C. Y. Lee, Conformational studies of novel estrogen receptor ligands by 1D and 2D NMR spectroscopy and computational methods, *Magn. Reson. Chem.*, 2003, **41**(4), 246–252.
41 C. P. Butts, C. R. Jones, E. C. Towers, J. L. Flynn, L. Appleby and N. J. Barron, Interproton distance determinations by NOE–surprising accuracy and precision in a rigid organic molecule, *Org. Biomol. Chem.*, 2011, **9**(1), 177–184.
42 C. R. Jones, C. P. Butts and J. N. Harvey, Accuracy in determining interproton distances using Nuclear Overhauser Effect data from a flexible molecule, *Beilstein J. Org. Chem.*, 2011, **7**(1), 145–150.
43 J. Keeler, *Understanding NMR Spectroscopy*, John Wiley & Sons, 2010.
44 A. B. Sebag, R. N. Hanson, D. A. Forsyth and C. Y. Lee, Conformational studies of novel estrogen receptor ligands by 1D and 2D NMR spectroscopy and computational methods, *Magn. Reson. Chem.*, 2003, **41**(4), 246–252.
45 H. Saito, I. Ando and A. Ramamoorthy, Chemical Shift tensor-the heart of NMR: Insight into biological aspects of proteins, *Prog. Nucl. Magn. Reson. Spectrosc.*, 2010, **57**, 181–228.
46 J. Ying, A. Grishaev, D. L. Bryce and A. D. Bax, Chemical Shift Tensors of Protonated Base Carbons in Helical RNA and DNA from NMR Relaxation and Liquid Crystal Measurements, *J. Am. Chem. Soc.*, 2006, **128**, 11443–11454.
47 Y. Wei, D. K. Lee and A. Ramamoorthy, Solid-state ^{13}C NMR Chemical Shift Anisotropy Tensors of polypeptides, *J. Am. Chem. Soc.*, 2001, **123**, 6118–6126.

Open Access Article. Published on 10 February 2026. Downloaded on 2/17/2026 2:53:54 PM.
This article is licensed under a Creative Commons Attribution-NonCommercial 3.0 Unported Licence.

48 A. M. Orendt and J. C. Facelli, Solid state effects on NMR chemical shifts, *Annu. Rep. NMR Spectrosc.*, 2007, **62**, 115–178.

49 R. K. Harris, R. E. Wasylishen and M. J. Duer, *NMR Crystallography*, Wiley, 2009.

50 N. F. Ramsey, Magnetic Shielding of Nuclei in Molecules, *Phys. Rev.*, 1950, **78**, 699–703.

51 N. F. Ramsey, Chemical effects in nuclear magnetic resonance and in diamagnetic susceptibility, *Phys. Rev.*, 1952, **86**, 243–246.

52 E. Vinogradov, P. K. Madhu and S. Vega, High-resolution proton solid-state NMR spectroscopy by phase-modulated Lee-Goldburg experiment, *Chem. Phys. Lett.*, 1999, **314**, 443–450.

53 E. Vinogradov, P. K. Madhu and S. Vega, Proton spectroscopy in solid state nuclear magnetic resonance with windowed phase modulated Lee-Goldburg decoupling sequence, *Chem. Phys. Lett.*, 2002, **354**, 193–202.

54 T. Migita, H. Itoh, H. Hamamoto and M. Inoue, Impact of tryptophan positional isomerism on physicochemical and biological properties: a case study using gramicidin A analogs, *JACS Au*, 2025, **5**, 5504–5511.

55 M. P. Nicholas, E. Eryilmaz, F. Ferrage, D. Cowburn and R. Ghose, Nuclear spin relaxation in isotropic and anisotropic media, *Prog. Nucl. Magn. Reson. Spectrosc.*, 2010, **57**, 111–158.

56 A. M. Orendt and J. C. Facelli, Solid state effects on NMR chemical shifts, *Annu. Rep. NMR Spectrosc.*, 2007, **62**, 115–178.

57 N. Tjandra, A. Szabo and A. D. Bax, Protein backbone dynamics and 15B chemical shift anisotropy from quantitative measurement of relaxation interference effects, *J. Am. Chem. Soc.*, 1996, **118**(29), 6986–6991.

58 P. Dais and A. Spyros, ^{13}C nuclear magnetic relaxation and local dynamics of synthetic polymers in dilute solution and in the bulk state, *Prog. Nucl. Magn. Reson. Spectrosc.*, 1995, **27**, 555–633.

 © 2026 The Author(s). Published by the Royal Society of Chemistry